Available online at www.sciencedirect.com
ScienceDirect
Ore Geology Reviews 32 (2007) 629–650
ORE GEOLOGY REVIEWS
www.elsevier.com/locate/oregeorev

Structural control and hydrothermal alteration at the BIF-hosted Raposos lode-gold deposit, Quadrilátero Ferrífero, Brazil

P.A. Junqueira [a,*], L.M. Lobato [b], E.A. Ladeira [c], E.J.M. Simões [d]

[a] *CPRM – Serviço Geológico do Brasil, Belo Horizonte, Av Brasil 1731, Funcionários, Belo Horizonte, Minas Gerais, 30140-002, Brazil*
[b] *Departamento de Geologia, IGC-CPMTC, Universidade Federal de Minas Gerais, Av Antônio Carlos 6627, Pampulha, Belo Horizonte, Minas Gerais, 31270-901, Brazil*
[c] *Geotecmin – Geologia e Tecnologia Mineral Ltda., Rua dos Aimorés 462/606, Funcionários, Belo Horizonte, Minas Gerais, 30140-070, Brazil*
[d] *FIEMG – Federação das Indústrias do Estado de Minas Gerais, Belo Horizonte, Av do Contorno, 4520, 8° andar, Funcionários, Belo Horizonte, Minas Gerais, 30110-090, Brazil*

Received 25 April 2004; accepted 29 March 2006
Available online 15 February 2007

Abstract

In the Raposos orogenic gold deposit, hosted by banded iron-formation (BIF) of the Archean Rio das Velhas greenstone belt, the hanging wall rocks to BIF are hydrothermally-altered ultramafic schists, whereas metamafic rocks and their hydrothermal schistose products represent the footwall. Planar and linear structures at the Raposos deposit define three ductile to brittle deformational events (D_1, D_2 and D_3). A fourth group of structures involve spaced cleavages that are considered to be a brittle phase of D_3. The orebodies constitute sulfide-bearing D_1-related shear zones of BIF in association with quartz veins, and result from the sulfidation of magnetite and/or siderite. Pyrrhotite is the main sulfide mineral, followed by lesser arsenopyrite and pyrite. At level 28, the hydrothermal alteration of the mafic and ultramafic wall rocks enveloping BIF define a gross zonal pattern surrounding the ore zones. Metabasalt comprises albite, epidote, actinolite and lesser Mg/Fe–chlorite, calcite and quartz. The incipient stage includes the chlorite and chlorite-muscovite alteration zone. The least-altered ultramafic schist contains Cr-bearing Mg-chlorite, actinolite and talc, with subordinate calcite. The incipient alteration stage is subdivided into the talc–chlorite and chlorite–carbonate zone. For both mafic and ultramafic wall rocks, the carbonate–albite and carbonate–muscovite zones represent the advanced alteration stage.

Rare earth and trace element analyses of metabasalt and its alteration products suggest a tholeiitic protolith for this wall rock. In the case of the ultramafic schists, the precursor may have been peridotitic komatiite. The Eu anomaly of the Raposos BIF suggests that it was formed proximal to an exhalative hydrothermal source on the ocean floor. The ore fluid composition is inferred by hydrothermal alteration reactions, indicating it to having been H_2O-rich containing CO_2+Na^+ and S. Since the distal alteration halos are dominated by hydrated silicate phases (mainly chlorite), with minor carbonates, fixation of H_2O is indicated. The CO_2 is consumed to form carbonates in the intermediate alteration stage, in halos around the chlorite-dominated zones. These characteristics suggest variations in the H_2O to CO_2-ratio of the sulfur-bearing, aqueous-carbonic ore fluid, which interacted at varying fluid to rock ratios with progression of the hydrothermal alteration.

Keywords: BIF-hosted gold; Archean greenstone belt; Hydrothermal alteration; Structural control; Quadrilátero Ferrífero; Brazil

* Corresponding author.
E-mail address: patricia@bh.cprm.gov.br (P.A. Junqueira).

0169-1368/$ - see front matter © 2007 Published by Elsevier B.V.
doi:10.1016/j.oregeorev.2006.03.004

1. Introduction

The Quadrilátero Ferrífero (QF), Minas Gerais State, Brazil, was the most important gold-producing region in Brazil from the early 18th Century until the late 1970s, and represents a world-class gold province. The most important lode-gold deposits (orogenic deposits as defined by Groves et al., 1998) are hosted by rocks of the Archean Rio das Velhas greenstone belt, and are located in the northern portion of this region. These include Morro Velho, Cuiabá, São Bento, Raposos, Faria, Bicalho, and Bela Fama (Fig. 1). Papers dealing with Morro Velho, Cuiabá and São Bento can be found elsewhere in the present volume (Vial et al., 200X; Ribeiro-Rodrigues et al., 200X; Martins Pereira et al., 200X, respectively).

The Raposos gold deposit, mined underground by Mineração Morro Velho Ltd., is situated in the northwestern portion of the QF, about 35 km SE of Belo Horizonte (Fig. 1). It was acquired in 1899 by the

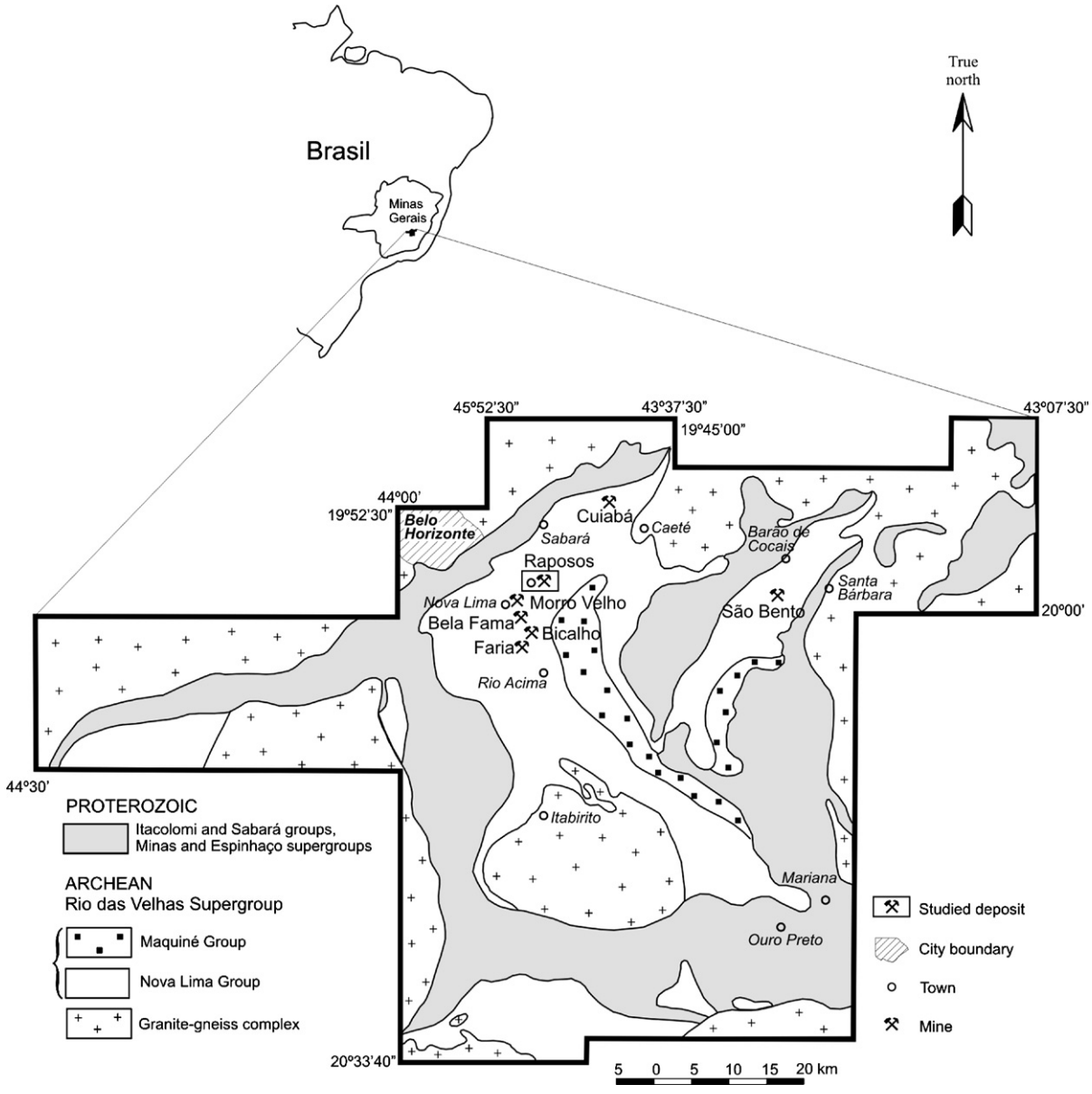

Fig. 1. Simplified geological map of the Quadrilátero Ferrífero region, showing the most important gold deposits (compiled from Dorr, 1969). The only operating mines at present are Cuiabá and São Bento.

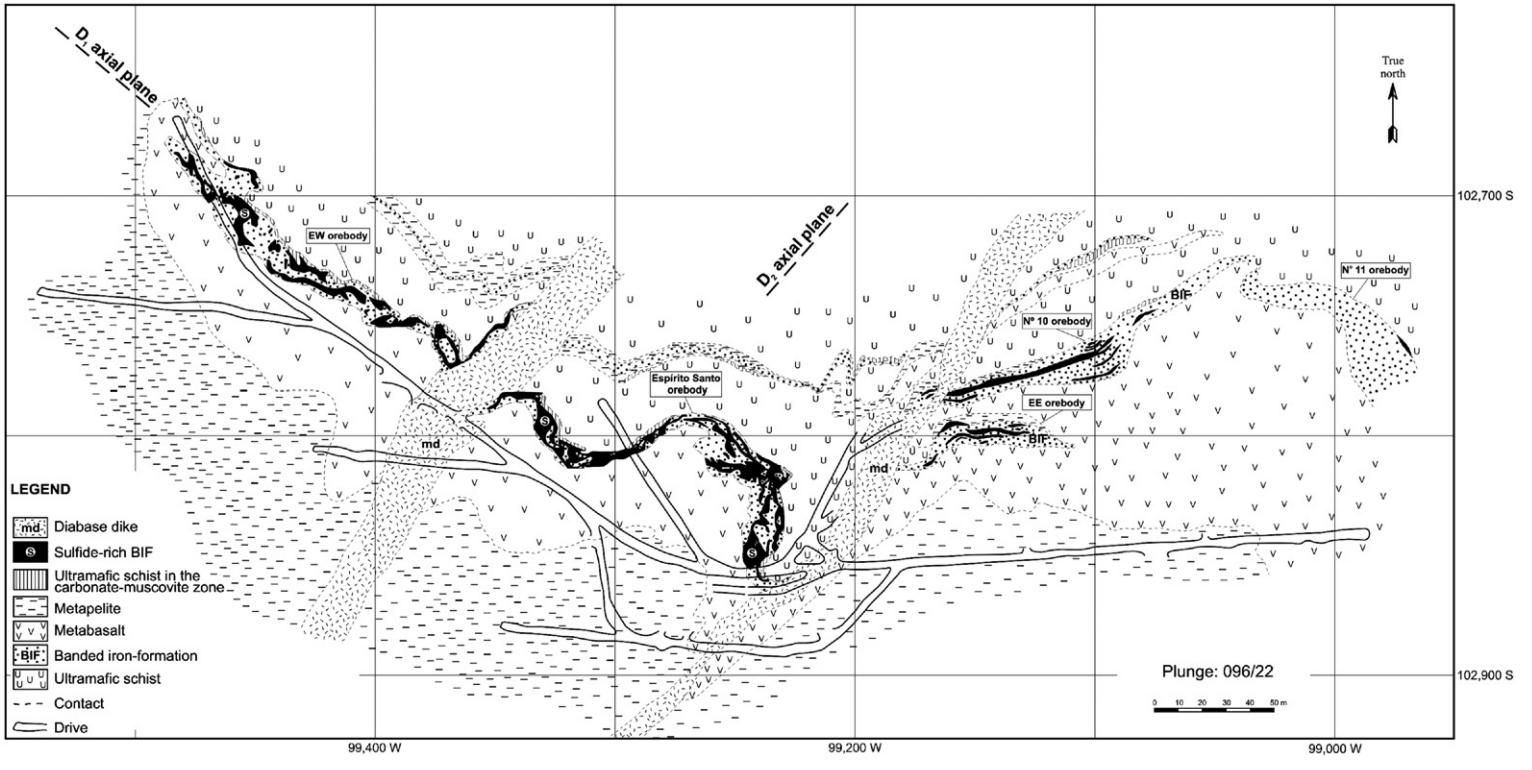

Fig. 2. Simplified geological map of the Raposos deposit, level 28 (modified from Junqueira, 1997).

British St. John Del Rey Mining Co., and sold in 1975 to Mineração Morro Velho S.A. The Raposos gold mine operated between 1920 and 1998, and when it was shut down over 10 Mt of gold ore had been extracted; *in situ* grades varied between 6.5 and 9.0 g/t Au.

Gold mineralization is associated with sheared, hydrothermally altered oxide–(±carbonate) facies BIF and is limited by envelopes of white mica-bearing schists in the foot- and hanging wall, respectively developed after ultramafic and mafic precursor schists (Vieira and Oliveira, 1988), and which represent proximal muscovite alteration zones (Fig. 2).

The deposit consists of 19 individual sulfide orebodies, with mineable areas from 100 to 1300 m^2, totaling 4000 m^2 that are distributed along the 1.6 km extent of banded iron-formation (BIF). Raposos was a deep (1423 m), mechanized mine, and exploitation took place by the cut-and-fill method with hydraulic fill. When it closed in May 1998, ore extraction was being carried out at levels 30 and 32 (1063 m depth), and mine development at levels 34 and 36 (1183 m depth). In 2002, the ore resource at Raposos stood at 3.39 Mt at an average grade of 6.97 g/t Au (Frederico W.R. Vieira, pers. comm., 2002).

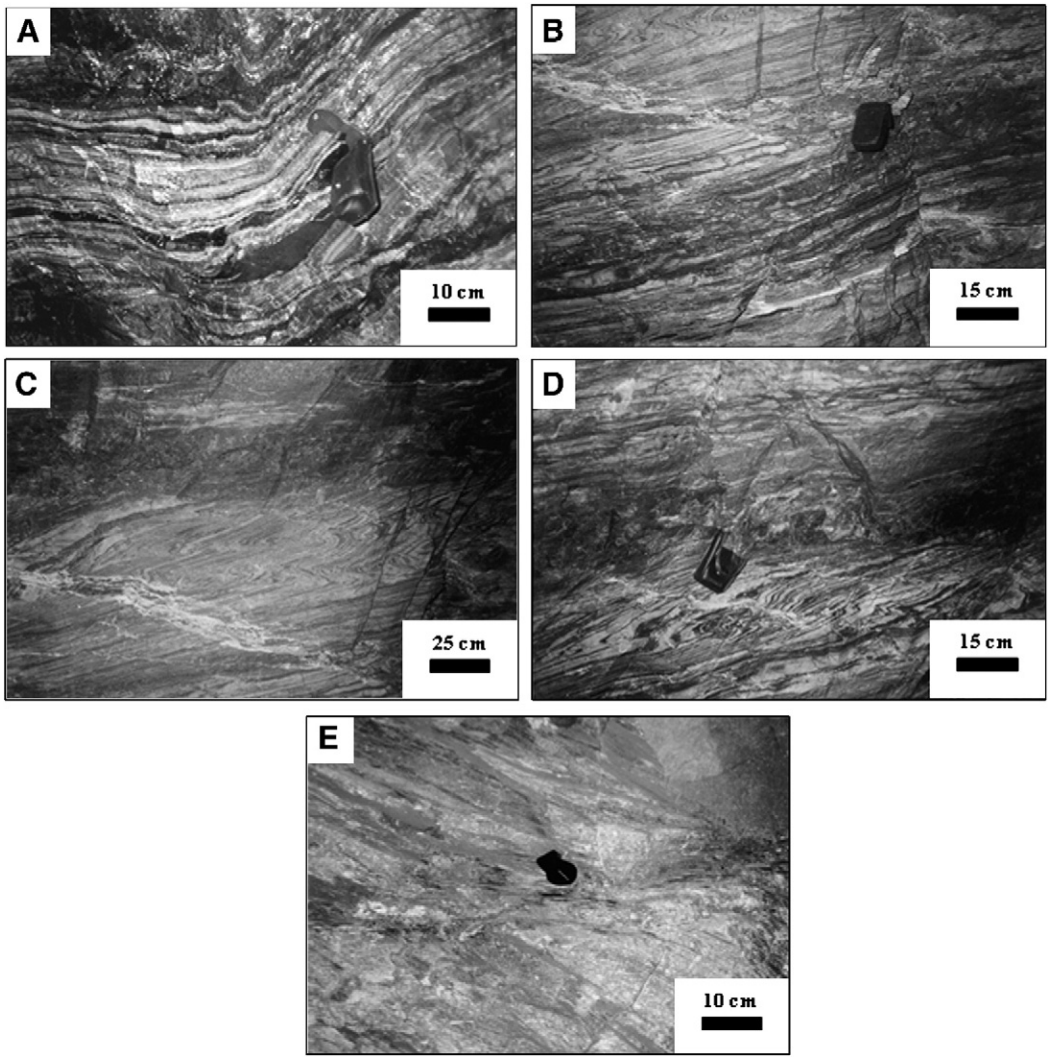

Fig. 3. Photographs of structural features of BIF. (A) Bedding (S_0) of BIF and S_1 schistosity parallel to S_0 (EW orebody, level 15). (B) D_1 shear band (the darkest portion), corresponding to the ore zone. Foliation S_2 is a spaced cleavage in BIF (EW orebody, level 15). (C) D_1 intrafolial folds. The ore zone is the darkest portion, where the bedding is completely destroyed (EW orebody, level 15). (D) Detailed view of a sheared/sulfidized zone (Espírito Santo orebody, level 24). (E) D_3 S-C foliations in a diabase dike indicating a clockwise movement (level 28).

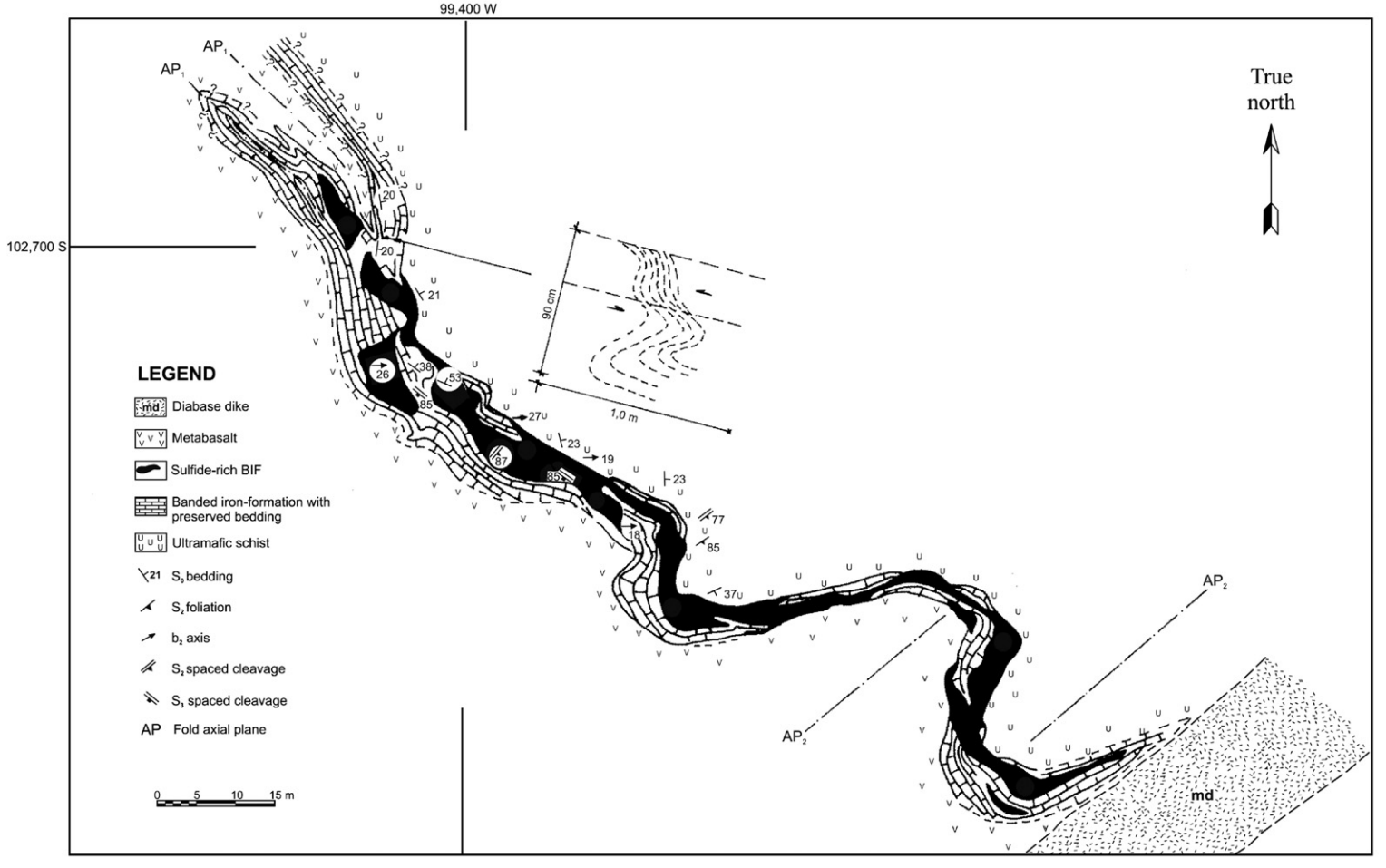

Fig. 4. Geological map of the Espírito West (EW) orebody, level 30 of the Raposos Mine (modified from Vieira and Simões, 1992).

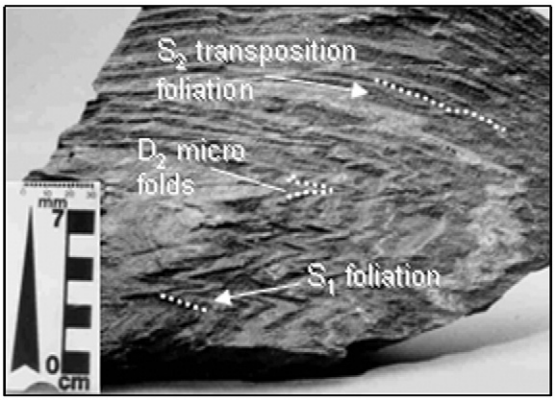

Fig. 5. Detail of hand sample of carbonaceous metapelite showing D_2 micro folds and S_1 foliation parallel to S_0. The foliation S_2 has a transposition character (level 28).

Vieira (1987a,b) gave pioneering detail about mineral assemblages related to the gold-associated hydrothermal alteration affecting rocks of the greenstone belt succession. Other notable contributions are those by Vieira (1988, 1991a) and Vieira and Simões (1992). Textural, mineralogical and chemical relationships have also been addressed by Ladeira (1980, 1985), Godoy (1994), Martins-Pereira (1995), Pereira (1996), Junqueira (1997) and Ribeiro-Rodrigues (1998), among others. The alteration and mineralization styles of selected gold deposits in the QF have been described and compiled by Lobato et al. (1998, 2001a).

This paper presents a description of the BIF-hosted, orogenic Raposos gold deposit and a model for structural control of ore emplacement. The main focus of the paper is the mineralogical and geochemical aspects

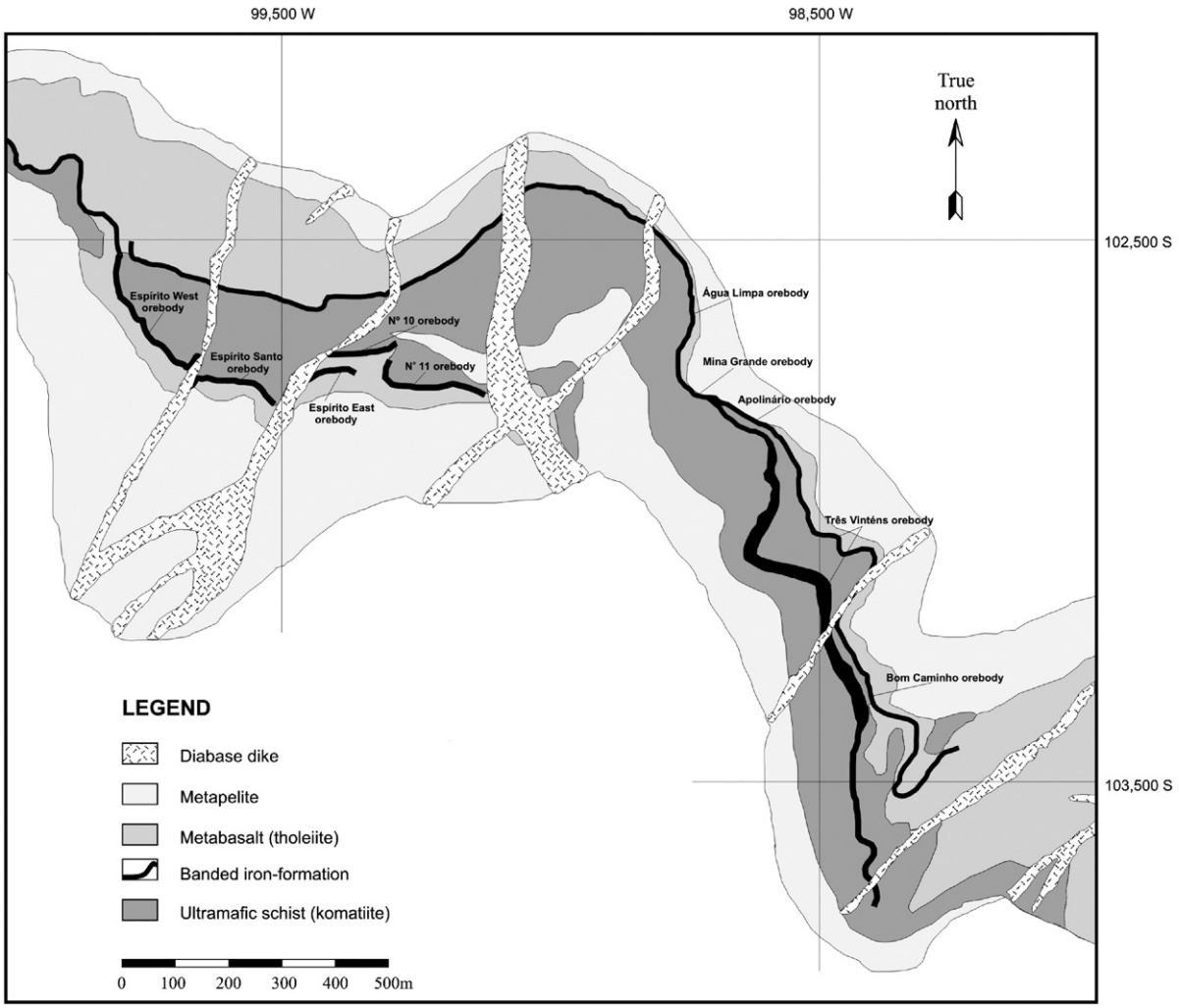

Fig. 6. Sketch geological map of the Raposos deposit, level 24, showing some of the main orebodies (modified from Vieira, 2000).

Table 1
Estimated percentage of sulfide content in selected thin sections of BIF, Espírito Santo orebody at levels 28 and 30 of the Raposos Mine

Thin section	Gq1-S18	3000-2	3000-3	Gq3-S18	Gq13-S11	Gq2-S18	3000-4
Pyrrhotite	3	1	14	_	5	5	7
Arsenopyrite	_	1	10	<1	1	4	2
Pyrite	_	<1	<1	2	2	1	1
Chalcopyrite	<1	_	1	<1	tr	<1	1
Au (ppm)	0.41	_	1.4	1.68	4.82	4.50	4.32

The amount of sulfides increases from left to right.
Note: in the thin section Gq13-S11, gold grains are included in pyrrhotite, carbonate and pyrite, whereas in Gq2-S18 finer gold grains are included in arsenopyrite.

of the mafic and ultramafic wall schists, with special emphasis on the alteration zoning, based mainly on the work by Junqueira (1997). In light of this integrated information a genetic model for the deposit is proposed.

2. Geological setting of the Raposos gold deposit

The Raposos gold deposit is associated with BIF of the Nova Lima Group, the basal section of the Rio das Velhas Supergroup (Vieira, 1987a), which hosts all the most important lode-gold deposits in the QF. The group comprises a classic greenstone succession, with ultramafic through mafic to intermediate volcanic rocks, and subordinate felsic volcanic rocks. Although there is no widely accepted stratigraphy for the Nova Lima Group as a whole (Dorr, 1969; Ladeira, 1980; Oliveira et al., 1983; Vieira and Oliveira, 1988; Ladeira, 1991; Baltazar and Pedreira, 1996), a review of earlier and newer data on the Rio das Velhas greenstone belt has been provided by Lobato et al. (2001b). Baltazar and Pedreira (1996) proposed a subdivision of the Nova Lima rocks based on lithofacies associations. The sequence displays mineral associations typical of the greenschist metamorphic facies. A new stratigraphic sequence of the Nova Lima Group is presented by Baltazar and Zucchetti (200X, this volume). The base of the Nova Lima Group encompasses mafic–ultramafic rocks, with massive, amygdaloidal, variolitic and locally pillowed metabasalts, intercalated with oxide facies banded iron formation, metachert, and carbonaceous schist; spinifex-textured peridotitic komatiites and cumulate sills can also display minor banded iron formation. Volcanoclastic rocks are represented by pyroclastic dacitic tuffs and agglomeratic horizons with minor lava flows. Volcanogenic and metasedimentary rocks show intercalations of felsic pyroclastic and epiclastic horizons (graywackes) with minor carbonaceous schist and carbonate schists. Metasedimentary rocks of mixed sources include quartz–mica–feldspar–chlorite, and carbonaceous schists (metapelites, metagraywackes and metapsammites).

Recent reviews of the geochronology of the Quadrilátero Ferrífero are presented by Noce (2001) and Lobato et al. (2001a,b). With regards to the Nova Lima Group and its gold deposits, these authors conclude that:

1. The evolution of the Rio das Velhas greenstone belt was associated with a major tectono-metamorphic and magmatic period at 2780–2700 Ma (Machado and Carneiro, 1992; Carneiro et al., 1998).
2. Mineralization must be older than the maximum age for the onset of Minas Supergroup sedimentation (2606±47 Ma; Machado et al., 1996), and was probably contemporaneous with or is older than minimum

Table 2
Electron microprobe analyses of chlorites from the Raposos metabasalts (Junqueira, 1997)

Sample number	GP-R901	GP-R901	ES1-S10	ES1-S10
	Pre-alteration zone		Chlorite-muscovite zone	
Chlorite	Ripidolite	Picnochlorite	Ripidolite	Ripidolite
SiO_2	26.64	26.69	27.41	25.88
TiO_2	n.d.	0.01	0.05	0.02
Al_2O_3	19.84	20.05	20.85	20.92
FeO	20.67	20.44	18.23	18.55
MnO	0.31	0.25	0.03	0.12
MgO	18.31	17.99	19.88	19.75
CaO	0.09	0.06	0.12	0.03
Na_2O	0.03	0.02	0.02	0.04
K_2O	0.06	0.03	n.d.	0.01
Cr_2O_3	0.10	0.15	0.23	0.23
Total	85.45	85.08	86.31	85.01
Cations on the basis of 36 <O,OH>				
Si	5.59	5.61	5.60	5.40
Al	4.91	4.96	5.02	5.14
Ti	n.d.	–	0.01	–
Fe	3.63	3.59	3.11	3.24
Mn	0.06	0.05	0.01	0.02
Mg	5.72	5.63	6.05	6.14
Ca	0.02	0.01	0.03	0.01
Na	0.01	0.01	0.01	0.02
K	0.02	0.01	n.d.	–
Cr	0.02	0.02	0.04	0.04
Total	19.97	19.89	19.86	20.00
Fe/(Fe+Mg)	0.39	0.39	0.34	0.35

Note: The average estimated H_2O content is 11 to 12%. n.d. not detected.
Classification after Hey (1954). The degree of hydrothermal alteration increases from left to right.

Pb–Pb model ages from the São Bento and Cuiabá deposits (2650 and 2670 Ma; DeWitt et al., 1994; Noce et al., 200X, this volume, respectively).

The numerous geochronological data available for the QF region, Noce (2001) and Noce et al. (200X, this volume, and references therein) also indicate that: (i) the granite–gneissic complexes derive from igneous protoliths older than 2900 Ma; (ii) three granitic magmatic episodes affected the region during the NeoArchean (at ca. 2780–2760 Ma, 2720–2700 Ma, and 2600 Ma); two felsic magmatic events associated with the greenstone belt sequence are separated in time (*ca*. 3030 Ma and 2772 Ma), the youngest constraining a major magmatic and tectonic event; (iii) although the main mineralization event for the gold deposits has not been dated unequivocally, the results known to date point to an age of 2700 Ma; (iv) Proterozoic Lake–Superior-type banded iron formations were deposited at ca. 2500–2400 Ma; (v) the eastern part of the QF was also affected by the Brasiliano Orogeny (600 to 560 Ma).

3. Mine-scale structures

Planar and linear structures at the Raposos deposit define three ductile to brittle deformational events namely D_1, D_2 and D_3. A fourth group of structures involve spaced cleavages that are considered to be a brittle phase of D_3 (Ladeira et al., 1991; Junqueira, 1997).

Structures assigned to D_1 include large-scale, ductile to ductile–brittle shear zones (SZ_1), mylonitic foliation, a stretching lineation and intrafolial folds and dislocated grains (Fig. 3A–C), typical mainly in the BIF. SZ_1 are bounded by hydrothermally altered, blastomylonitic schists, which are 200 m thick and more than 3 km wide. These are the most important structures of the deposit, since they are interpreted to relate to both the hydrothermal alteration and the gold mineralization. The F_1 folds are tight, with E–W hinge lines parallel to the stretching lineation (L_1), which plunges from 30 to 12° (at 1400 m depth) towards east. The folds form type-3 interference patterns of Ramsay (1967). At level 30, the geological map of the Espírito West orebody displays a relict F_1 fold in the western extremity (Fig. 4). The axial-planar foliation, S_1, is parallel to the bedding (S_0) of both BIF and metapelites, and dips from 035 to 120 at between 25 and 40° (Fig. 5). The foliation S_1 develops a mylonitic or transposition character in highly deformed zones. Shear zones SZ_1 are roughly parallel to S_1 and destroy the BIF S_0, which is preserved only in elongated relics within shear zones (Fig. 3A).

D_2 is defined by inclined similar folds verging towards north, which collectively form a major inclined and overturned fold that defines the shape of the deposit (Figs. 4 and 6). The axial-planar, NE-striking S_2 foliation dips towards 120 to 150° at between 45° at surface, and 12° at level 44 (1430 m depth); it is a

Table 3
Electron microprobe analyses of carbonates from the Raposos metabasalts (Junqueira, 1997)

Sample number	GP-R901	GP-R901	2,3-10A	2,3-10A	ES1-S10	GP17-S1	GP17-S1	GP17-S1	GP4-S18
	Pre-alteration zone		Chlorite–muscovite zone		Chlorite–muscovite zone	Carbonate-albite zone			Carbonate-albite zone
Carbonate	Calcite	Calcite	Ankerite	Ankerite	Calcite	Ankerite ferroan	Ankerite ferroan	Siderite magnesian	Ankerite
$Fe(CO_3)$	0.78	0.62	17.97	19.45	1.18	21.46	24.56	66.98	19.88
$Mn(CO_3)$	0.96	0.79	1.05	1.12	0.76	0.73	0.71	1.27	1.03
$Mg(CO_3)$	0.47	0.38	26.94	25.58	1.19	24.9	22.86	30.13	24.92
$Ca(CO_3)$	97.80*	98.22*	52.38	51.99	96.86	52.19	50.75	0.49	52.36
Total	100	100	98.34	98.14	99.98	99.29	98.88	98.87	98.19
Cations on the basis of 6 <O>									
Mg	0.01	0.01	0.63	0.61	0.03	0.58	0.54	0.75	0.59
Fe	0.01	0.01	0.31	0.34	0.02	0.37	0.42	1.21	0.34
Mn	0.01	0.01	0.02	0.02	0.01	0.01	0.01	0.02	0.02
Ca	1.97*	1.96	1.04	1.04	1.93	1.03	1.01	0.01	1.04
Total	2.00	1.99	2.00	2.00	2.00	1.99	1.99	1.99	2.00

Classification of carbonate after Deer et al. (1966). The degree of hydrothermal alteration increases from left to right.
Note: * values recalculated to 100% – or to the total of the cations – since some results of this element were overestimated during the analyses.

Table 4
Electron microprobe analyses of chlorites from the Raposos ultramafic schists (Junqueira, 1997)

Sample number	2,3-11	GP14-S11	GP14-S11	GP14-S11	GP14-S11	2,3-6	2,3-6	2,3-6	2,3-6	2,3-6	2,3-4B	GP5-S18	GP5-S18
	Pre-alteration zone	Talc–chlorite zone				Talc–chlorite zone					Carbonate–albite zone	Carbonate–muscovite zone	
Chlorite	Ripidolite	Picnochlorite	Picnochlorite	Picnochlorite	Picnochlorite	Picnochlorite	Picnochlorite	Picnochlorite	Picnochlorite	Ripidolite	Ripidolite	Ripidolite	Ripidolite
SiO_2	26.71	28.06	28.76	27.92	28.67	28.18	27.73	27.65	28.60	27.70	26.09	23.76	24.42
TiO_2	n.d.	0.02	0.03	0.03	0.03	0.05	0.04	0.01	0.03	0.04	0.03	0.09	0.06
Al_2O_3	18.58	19.43	18.66	19.00	18.43	18.40	18.35	19.10	17.22	20.26	18.53	20.07	19.88
FeO	14.32	13.63	13.85	13.41	13.34	15.16	15.07	14.73	14.82	14.10	16.63	28.84	27.74
MnO	0.12	0.02	0.05	0.02	0.05	0.08	0.06	0.06	0.06	0.10	0.09	0.06	0.06
MgO	22.91	23.69	24.14	24.45	24.48	23.10	23.01	22.57	23.15	22.78	20.94	12.38	12.56
CaO	0.01	0.05	0.01	0.01	0.03	0.04	0.08	0.01	0.08	0.08	0.01	0.02	0.07
Na_2O	0.02	0.02	0.01	0.02	0.03	0.02	n.d.	n.d.	0.03	0.01	0.01	0.02	0.03
K_2O	0.02	0.02	0.06	0.02	0.03	0.03	n.d.	0.01	0.02	0.04	0.01	n.d.	0.01
Cr_2O_3	0.85	0.96	0.83	0.90	0.77	0.93	1.31	1.18	1.87	1.08	1.63	0.02	0.83
NiO	0.15	0.06	0.10	0.05	0.07	0.11	0.06	0.10	0.04	0.11	0.13	0.07	0.07
Total	83.70	85.94	86.50	85.83	85.93	86.09	85.70	85.42	85.92	86.29	84.10	85.32	85.73
Cations on the basis of 36 <O,OH>													
Si	5.595	5.674	5.782	5.653	5.788	5.743	5.684	5.667	5.845	5.597	5.525	5.285	5.376
Al	4.59	4.63	4.42	4.53	4.39	4.42	4.43	4.62	4.15	4.82	4.62	5.26	5.16
Ti	n.d.	n.d.	0.01	n.d.	n.d.	0.01	0.01	n.d.	0.01	0.01	0.01	0.02	0.01
Fe	2.51	2.31	2.33	2.27	2.25	2.58	2.58	2.53	2.53	2.38	2.95	5.36	5.11
Mn	0.02	n.d.	0.01	n.d.	0.01	0.01	0.01	0.01	0.01	0.02	0.02	0.01	0.01
Mg	7.15	7.14	7.23	7.38	7.37	7.02	7.03	6.90	7.05	6.86	6.61	4.11	4.12
Ca	n.d.	0.01	n.d.	n.d.	0.01	0.01	0.02	n.d.	0.02	0.02	n.d.	0.01	0.02
Na	0.01	0.01	0.01	0.01	0.01	0.01	n.d.	n.d.	0.01	n.d.	n.d.	0.01	0.01
K	0.01	0.01	0.02	0.01	0.01	0.01	n.d.	n.d.	n.d.	0.01	n.d.	n.d.	n.d.
Cr	0.14	0.15	0.13	0.14	0.12	0.15	0.21	0.19	0.30	0.17	0.27	n.d.	0.14
Ni	0.03	0.01	0.02	0.01	0.01	0.02	0.01	0.02	0.01	0.02	0.02	0.01	0.01
Total	20.05	19.94	19.95	20.01	19.97	19.97	19.99	19.93	19.94	19.91	20.02	20.07	19.97
Fe/(Fe+Mg)	0.26	0.24	0.24	0.24	0.23	0.27	0.27	0.27	0.26	0.26	0.26	0.24	0.24

Classification of chlorite based on Hey (1954). The degree of hydrothermal alteration increases from left to right.
Note: The average estimated H_2O content is 11 to 12%. %. n.d. not detected.

transposition foliation in schists (Fig. 5), and a spaced cleavage in BIF (Fig. 3B). The hinge lines, b_2 and b_1, are grossly coaxial and parallel to mineral and stretching lineations. F_2 folds are generated by shearing as defined by drag folds at the extremities of the Espírito West and Espírito Santo orebodies (Fig. 2). These shear zones are ductile (in schists) or ductile to ductile–brittle (in BIF) and are roughly parallel to S_2. The trend of diabase dikes that crosscut the orebodies is also parallel to S_2. The dikes display S_2 schistosity along their borders, suggesting that their emplacement occurred during the late stages of D_2.

The D_3 event occurred in the brittle–ductile regime and generated shear zones (SZ_3), spaced and crenulation cleavages (S_3), and lineations (L_3). The SZ_3 shear zones trend N–S/15° E (C foliation) and are common in both schists and diabase dikes (Fig. 3E). A decrease in S_2 and L_2 dip values down plunge with depth suggests a thrust ramp. The S-C foliations indicate tectonic transport from east to west. The S_3 foliation has an N–S trend and dips between 70° and 90° to WSW. Gravity step faults that are parallel to S_3 are common and displace the orebodies, with small net slips. The crenulation of S_2 and the intersection lineations between S_3 and S_2 or S_1 generate L_3. North–S and E–W subvertical, spaced cleavages and joints overprint D_3 structures and are considered to represent a late structural phase.

4. Gold mineralization in the Raposos deposit

Several publications address the geology and mineralization at the Raposos gold deposit, e.g., Tolbert (1964), Vial (1980), Ladeira (1980), Vieira (1987a,b, 1988, 1991a,b,c), Ladeira et al. (1991), Vieira and Simões (1992), Godoy (1994), Junqueira (1997) and Lobato et al. (1998).

Gold mineralization is associated with sulfidized BIF, which is limited by envelopes of white micaceous schists in the foot- and hanging wall, respectively developed after ultramafic and mafic precursor schists (Vieira and Oliveira, 1988). The non-deformed and unaltered Raposos BIF studied at level 28 displays alternate layers of fine-grained granoblastic siderite, ankerite and rarely, magnetite and quartz. Where sulfide minerals are present, pyrrhotite is the dominant phase. Non-mineralized BIF, with segments in which S_0 is preserved, has an average gold grade of 2.5 g/t.

All orebodies constitute sulfide-bearing SZ_1 shear zones of BIF (Fig. 3B, D), except the Ouro Preto orebody which is associated with quartz boudins hosted by talc schist. Orebodies hosted in BIF result from the replacement of magnetite and/or siderite. Gold-bearing

Table 5
Electron microprobe analyses of carbonates from the Raposos ultramafic schists (Junqueira, 1997)

Sample number	2,3-11	2,3-11	2,3-11	GP14-S11		GP14-S11	GP14-S11	GP14-S11	2,3-6	2,3-6	2,3-6	2,3-4B		2,3-4B	GP5-S18		GP5-S18
	Pre-alteration zone			Talc–chlorite zone					Talc–chlorite zone			Carbonate–albite zone			Carbonate–muscovite zone		
Carbonate	Calcite	Calcite	Calcite	Dolomite		Dolomite	Dolomite	Dolomite	Calcite	Calcite	Calcite	Calcite	Ankerite	Ankerite	Ankerite	Ankerite ferroan	Ankerite
$Fe(CO_3)$	0.98	0.90	0.94	9.37		9.07	8.50	9.05	1.41	1.72	1.29	14.1		11.62	21.31		17.32
$Mn(CO_3)$	0.99	0.88	0.79	1.10		1.18	1.24	1.24	0.78	0.78	0.83	1.07		0.94	1.09		0.60
$Mg(CO_3)$	1.44	1.35	1.08	35.77		35.41	37.12	36.45	1.91	1.88	1.54	30.58		33.5	24.98		28.18
$Ca(CO_3)$	96.59*	95.42	94.73	52.37		52.46	53.28	51.97	95.90*	95.63*	97.83	51.54		51.43	51.48		52.49
Total	100	98.55	97.53	98.60		98.11	100.14	98.71	100	100	101.50	97.29		97.48	98.86		98.59
Cations on the basis of 6 <O>																	
Mg	0.03	0.03	0.03	0.82		0.81	0.83	0.83	0.04	0.04	0.04	0.72		0.78	0.59		0.66
Fe	0.02	0.02	0.02	0.16		0.15	0.14	0.15	0.02	0.03	0.02	0.24		0.20	0.37		0.30
Mn	0.02	0.02	0.01	0.02		0.02	0.02	0.02	0.01	0.01	0.01	0.02		0.02	0.02		0.01
Ca	1.93	1.93	1.94	1.01		1.02	1.01	1.00	1.91	1.91	1.92	1.02		1.01	1.02		1.03
Total	2.00	2.00	2.00	2.00		2.00	2.00	2.00	1.99	1.99	2.00	2.00		2.00	2.00		2.00

Note * values recalculated to 100% – or to the total of the cations – since some results of this element were overestimated during the analyses.
Classification of carbonate based on Deer et al. (1966). The degree of hydrothermal alteration increases from left to right.

zones of varying sulfide composition are laterally continuous, having a pseudo-stratiform appearance, many being parallel or slightly oblique to shear quartz veins (Fig. 3D). Gold grades are positively correlated with the amounts of sulfide in the rock. Pyrrhotite is the main sulfide mineral, followed by lesser amounts of arsenopyrite and pyrite (Table 1). Gold occurs as anhedral grains or films along fractures in sulfides. When associated with pyrrhotite, gold is relatively coarse (in the 50 to 120 μm range), and occurs mainly along grain boundaries. When occurring as inclusions in pyrite, gold grains vary from 10 to 50 μm in size; where included in arsenopyrite or associated with gangue minerals, gold is generally finer (<10 μm). An abundance of finer-grained pyrrhotite correlates with higher gold grades of up to 60 to 80 g/t Au; Au:Ag ratios range from 8:1 to 5:1.

The largest orebodies in the area and the highest gold grades are on the north limb of the major D_2 fold. These are the Espírito West (900 m^2 with 7.56 g/t); Espírito Santo (1500 m^2, 7.30 g/t); N°10 (450 m^2, 5.5 g/t Au) and N°11 orebodies. The Mina Grande orebody occupies a hinge zone, and has the highest grade (286 m^2, 12.8 g/t Au); it was the only orebody where the non-altered oxide-facies BIF could be seen during the present underground study. The southern limb has lower grade, smaller orebodies, such as Apolinário, Água Limpa, Três Vinténs and Bom Caminho (Fig. 6).

The down-plunge extensions of the orebodies are characterized by decreasing gold grades. This is the case for orebody N°11 at level 24 (823 m depth), Mina Grande at level 26 (883 m) and N°10 at level 30. The EW and Espírito Santo orebodies have a significant drop in gold grade between levels 30 and 32 (from 7.5 g/t to 5.5 g/t Au) and levels 32 and 34 (1123 m), respectively. In all of these cases, SZ_1 shear zones are either absent or rare.

The wall rocks of the BIF are ultramafic schist in the north, and mafic and carbonaceous schists in the south. The hanging wall ultramafic schist is derived from peridotitic komatiites, whereas the footwall metamafic rock from tholeiitic basalt. The least hydrothermally altered ultramafic and mafic rocks are represented by

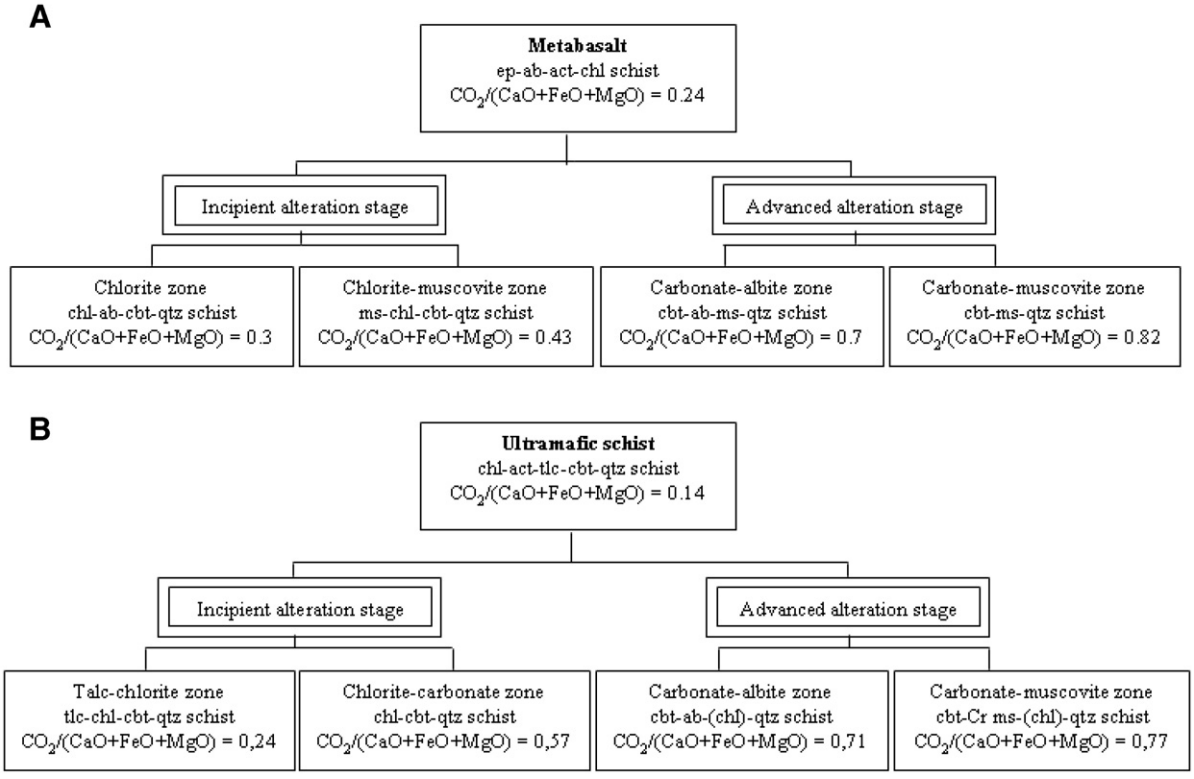

Fig. 7. Schematic diagram showing the rock types derived from A) metabasalt, and B) ultramafic schist in the incipient and advanced stages of hydrothermal alteration to the Raposos deposit (after Junqueira, 1997). Abbreviations: act — actinolite; ab — albite; cbt — carbonate; chl — chlorite; Cr ms — (Cr)-muscovite; ep — epidote; ms — muscovite; qtz — quartz; tlc — talc.

chlorite–actinolite–talc–calcite and epidote–albite–actinolite–chlorite (±calcite) schists, respectively. Quartz–carbonate–muscovite schist with carbonaceous matter is interpreted to be a metapelite. Diabase dikes crosscut all these rocks (Fig. 2).

5. Hydrothermal alteration

Junqueira (1997) investigated the hydrothermal alteration of the metamorphosed mafic and ultramafic wallrocks enveloping BIF at level 28 (Fig. 2). Despite a complex distribution of alteration zones, geological mapping, combined with petrography and whole-rock geochemistry indicate that most rock units contain metamorphic minerals that have been replaced by hydrothermal assemblages that define a gross zonal pattern surrounding the ore zones. Tables 2–5 report electron microprobe analyses of chlorites and carbonates of both mafic and ultramafic rocks. Analytical data were obtained on a CAMECA Camebax SX-50 electron microprobe at the Instituto de Geociências da Universidade de Brasília-UnB, using a 15 kV voltage and a 25 nA current.

The boundaries between alteration zones may be knife sharp, or gradational over the cm- to m-scale. Sharp boundaries are common in proximal alteration

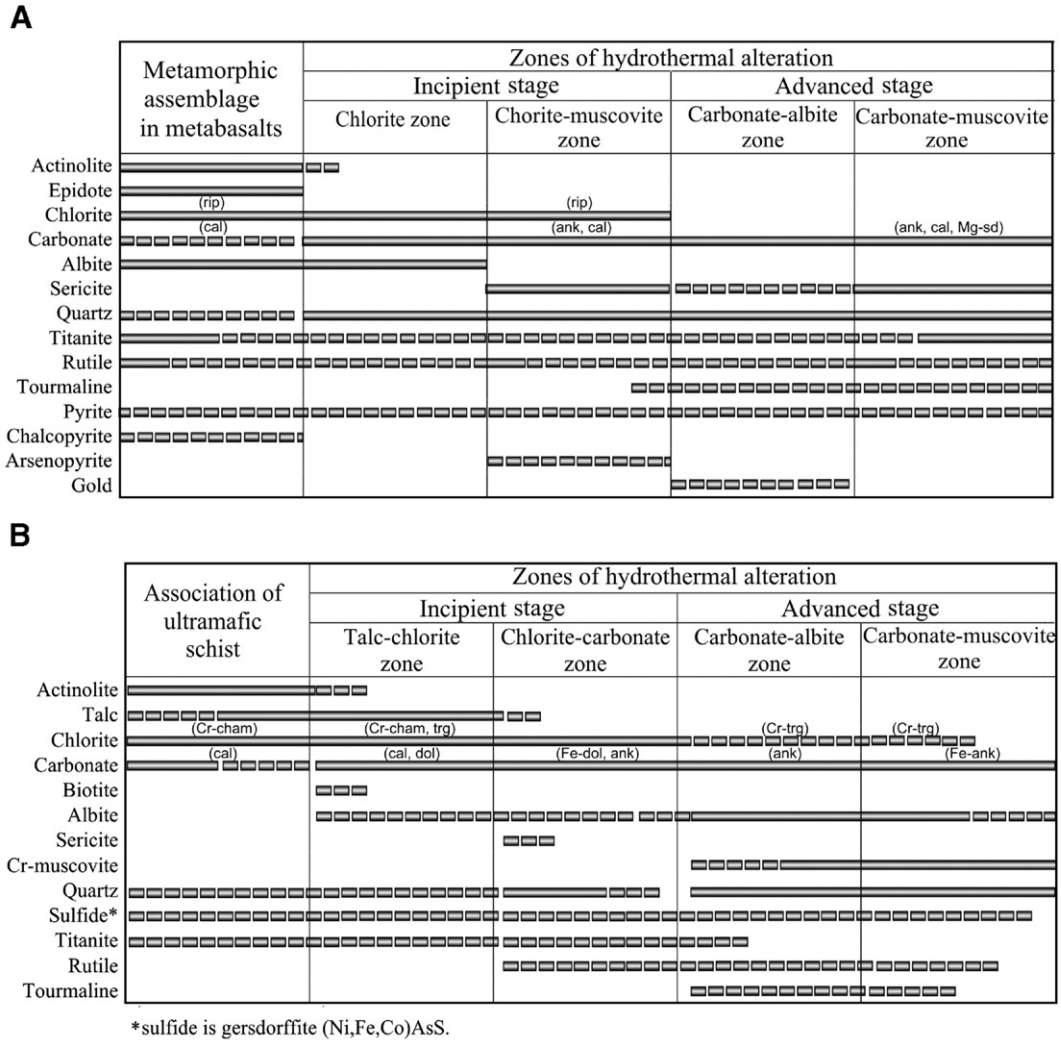

Fig. 8. Mineralogical changes involved in the hydrothermal alteration of A) metabasalt and B) ultramafic schist at the Raposos deposit (data from Junqueira, 1997). Abbreviations: ank — ankerite; cal — calcite; Cr-cham — (Cr)-chamosite; Cr-trg — (Cr)-thuringite; dol — dolomite; Fe-ank — (Fe)-ankerite; Fe-dol — (Fe)-dolomite; Mg-sd — (Mg)-siderite; rip — ripidolite; trg — thuringite.

zones, whereas diffuse boundaries predominate in distal alteration zones, which grade into the least-altered regional metamorphic assemblages.

Incipient (buffered) and advanced (unbuffered) alteration stages are distinguished by Junqueira (1997), and represent the distal and proximal alteration halos. Each stage encompasses two alteration zones, adding more detail to the scheme previously suggested by Vieira (1988). The mineralogical characteristics of the incipient stage are specific to each lithological type. Both carbonate–albite and carbonate–muscovite alteration zones are characteristic and attributed to the advanced stage of hydrothermal alteration (Figs. 7 and 8).

5.1. Metabasalts

The pre-hydrothermal alteration D_1-related metamorphic assemblage in metabasalt comprises albite, epidote, actinolite and lesser Mg/Fe-chlorite, calcite and quartz; pyrite and chalcopyrite are accessory minerals. Fine-grained albite (ca. 30 to 40%) occurs in the matrix and is interpreted to have been generated by spilitization, as originally described by Ladeira (1980) for the Nova Lima Group.

The incipient alteration stage is subdivided into the chlorite and chlorite–muscovite zones, which are marked by the disappearance of both epidote and actinolite. These reactions (Table 6, reaction I) involve the development of chlorite and calcite from epidote + actinolite (Fig. 9A, B), giving way to a chlorite–albite–carbonate (calcite and ankerite)–quartz schist. The chlorite–muscovite zone is marked by the replacement of the albite + chlorite + calcite assemblage to form a muscovite–chlorite–carbonate (ankerite)–quartz schist, by way of interaction with $CO_2 + K^+$. This $CO_2 + K^+$-rich fluid stage probably evolved into a $H_2O + Na^+$ fluid (Table 6, reaction II).

The carbonate–albite and carbonate–muscovite zones represent the advanced alteration stage. The former characterizes carbonate–albite–muscovite–quartz schist formed by the nucleation of hydrothermal albite associated with Fe-ankerite/Mg-siderite at the expense of chlorite + calcite + quartz, reflecting reaction with $CO_2 + Na^+$ (Table 6, reaction III). In the carbonate–muscovite zone, chlorite + calcite can also be replaced by an Mg-siderite + muscovite + quartz assemblage, probably attained through interaction with $CO_2 + K^+$, with H^+ release (Table 6, reaction IV). There is pronounced Fe enrichment in carbonates, ranging from calcite in metabasalt to Fe-ankerite and Mg-siderite with increasing degrees of alteration. The Fe:Mg ratio of chlorites also increases, ranging from 0.61 to 0.66.

Table 6
Chemical reactions suggested to represent the main changes involved in the hydrothermal alteration of metabasalts and ultramafic schists, for each alteration zone of the Raposos deposit (adapted following the scheme by Colvine et al., 1988)

A) Metabasalt
Incipient alteration stage
Chlorite zone
(I) 2 epidote + 3 actinolite + 10 CO_2 + 6 H_2O → 3 chlorite + 10 calcite + 21 quartz + 13 O_2
Chlorite–muscovite zone
(II) albite + chlorite + 5 calcite + 5 CO_2 + K^+ → muscovite + 5 ankerite + 3 quartz + 3 H_2O + Na^+
Advanced alteration stage
Carbonate–albite zone
(III) chlorite + 5 calcite + 3 quartz + 5 CO_2 + 2 Na^+ → 5 ferroan ankerite + 2 albite + 3 H_2O + 2 H^+
Carbonate–muscovite zone
(IV) 3 chlorite + 15 calcite + 24 CO_2 + 2 K^+ → 2 muscovite + 15 magnesian siderite + 3 quartz + 9 H_2CO_3 + 2 H^+
B) Ultramafic schists
Incipient alteration stage
Talc–chlorite zone
(V) 2 serpentine + actinolite + anorthite + 6 CO_2 → Fe–talc + Mg (Fe)–chlorite + 3 Fe–dolomite + 7 quartz
Chlorite–carbonate zone
(VI) Fe–talc + 3 calcite + 3 CO_2 → 3 ankerite + 4 quartz + H_2O
(VII) titanite + CO_2 → rutile + calcite + quartz
Advanced alteration stage
Carbonate–albite zone
(VIII) Mg (Fe)–chlorite + 5 calcite + 3 quartz + 5 CO_2 + 2 Na^+ → 5 ankerite + 2 albite + 3 H_2O + 2 H^+
Carbonate–muscovite zone
(IX) Mg (Fe)–chlorite + albite + 5 calcite + 5 CO_2 + K^+ → Cr–muscovite + 5 ferroan ankerite + 3 quartz + 3 H_2O + Na^+

5.2. Ultramafic schists

In the mine area, these rocks rarely preserve the metamorphic mineralogy, with the least-altered examples containing Cr-bearing Mg-chlorite, actinolite and talc, with subordinate calcite (Fig. 9). In other parts of the Nova Lima Group, rocks with serpentine, clino- and orthopyroxenes and pseudomorphs after olivine have been described by Vieira (1991a).

The incipient alteration stage is subdivided into the talc-chlorite and chlorite–carbonate zones, which are characterized by the formation of chlorite–carbonate–quartz schists with or without varying amounts of talc. Chlorite contains a small amount of Cr (0.15 to 0.3 atoms per formula unit) and talc contains an average of 0.6 a.p.f.u. Fe. Proposed mineral reactions involve the substitution of serpentine + actinolite + anorthite by Fe–

talc + Mg (Fe)–chlorite + Fe–dolomite + quartz (Fig. 9C, D), via interaction with CO_2 in the talc–chlorite zone (Table 6, reaction V). Further carbonate (ankerite) + quartz develops at the expense of talc + calcite, in the chlorite–carbonate zone (Table 6, reaction VI). The development of rutile + calcite + quartz from titanite is also diagnostic of this zone (Table 6, reaction VII).

The advanced alteration stage produced a carbonate-rich schist, with or without varying amounts of albite, chlorite and green mica, generically named fuchsite. The presence of fuchsite in Raposos (Cr-muscovite, with 0.7 to 1.3% Cr_2O_3) was originally described by Tolbert (1964), and its chemistry is detailed by Ladeira (1980). The formation of ankerite–albite ± chlorite ±

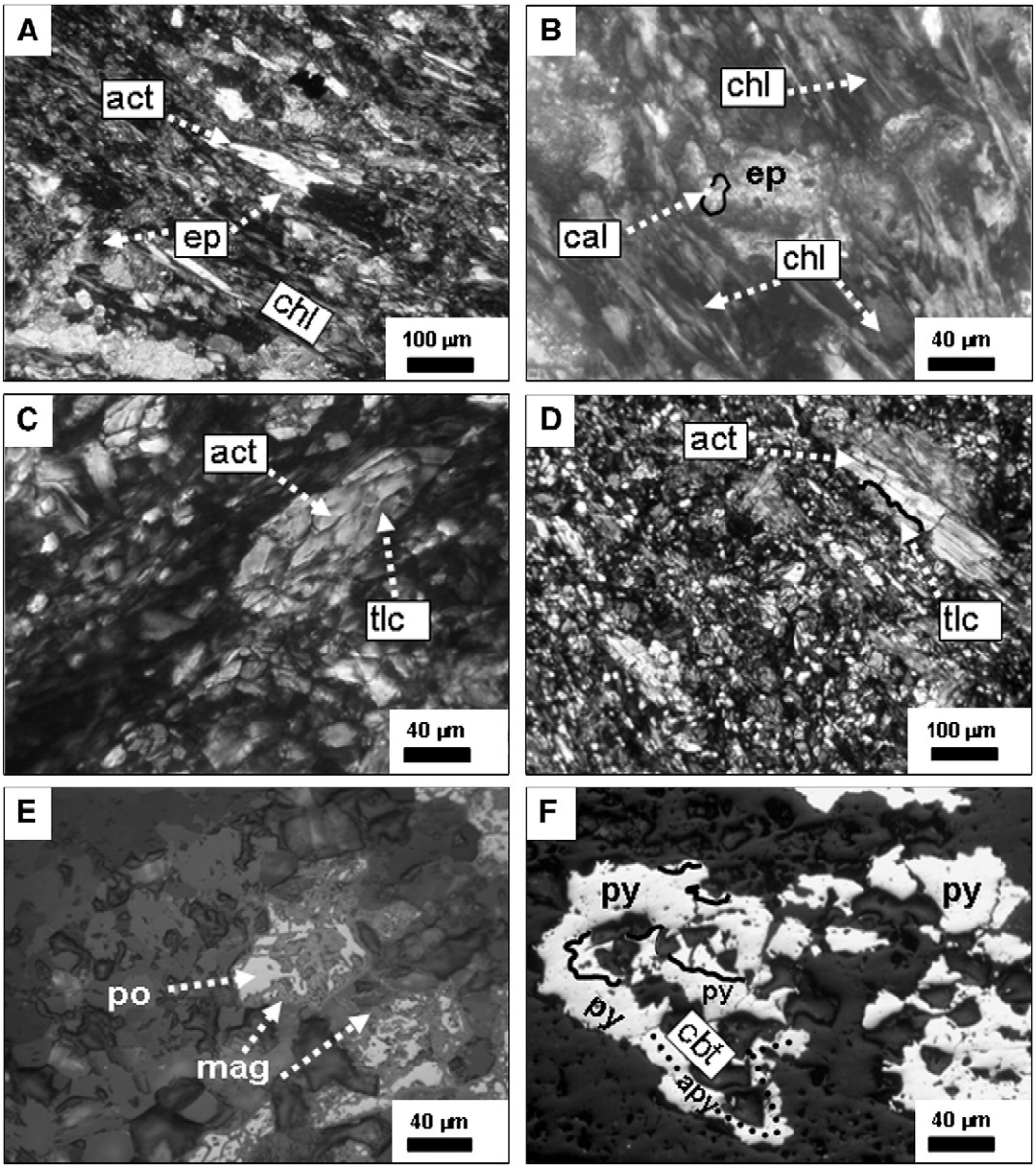

Fig. 9. Photomicrographs. (A) Least-altered metamafic rock, typical of the incipient alteration stage, showing the development of chlorite (chl) after actinolite (act) and epidote (ep). (B) as (A), also with the development of calcite (cal). (C) Least-altered ultramafic schist, with talc (tlc) and chlorite developed after actinolite (act), and typical of the talc–chlorite zone. (D) as (C), with actinolite lath partially replaced by talc. (E) Sulfidized BIF, with pyrrhotite (po) replacing magnetite (mag) that maintains its original habit. (F) as (E), with intergrown pyrite (py) and arsenopyrite (apy) developed after calcite; black lines mark the presence of apy growing at the expense of py.

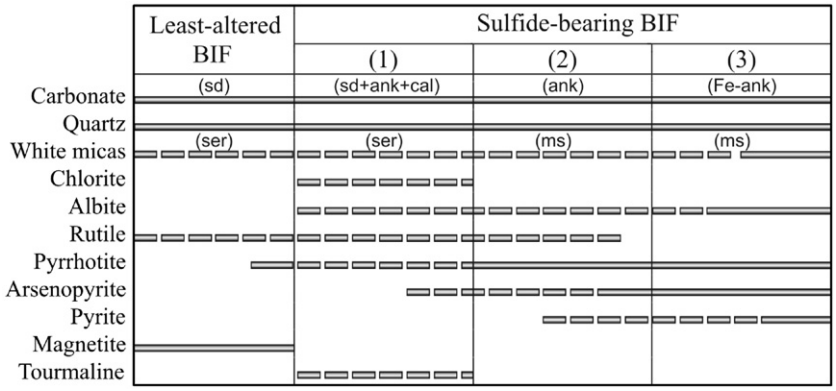

Fig. 10. Mineralogical composition of least-altered BIF, and its zones of progressive, hydrothermal-sulfide enrichment and shearing, Raposos gold deposit. Percentage of sulfide increases from (1) to (3). Gold grade increases from left to right (after Lobato et al., 1998). Abbreviations: ank — ankerite; cal — calcite; Fe-ank — (Fe)-ankerite; ms — muscovite; sd — siderite; ser — sericite.

Cr–muscovite–quartz schist in the carbonate–albite zone can be envisaged through the replacement of chlorite+calcite+quartz by ankerite+albite, where chlorite was partially to totally consumed to form carbonate and albite; the reaction involved CO_2+Na^+ consumption, with H^+ release (Table 6, reaction VIII). Finally, the carbonate–Cr muscovite schist represents the replacement of chlorite+albite+calcite to form ferroan ankerite+Cr–muscovite+quartz in the carbonate–muscovite zone; the reaction must have involved CO_2+K^+ consumption, with H_2O+Na^+ release (Table 6, reaction IX).

The main difference between the advanced alteration stages of the metabasalt and ultramafic schists is that the 'fuchsitic' green mica is characteristic of the latter, and chlorite may also be present.

Lobato and Vieira (1998) undertook an investigation of the mineralogical changes experienced by BIF during shearing and associated hydrothermal alteration and/or gold mineralization (Fig. 10). Non-deformed and unaltered BIF displays alternate layers of fine-grained granoblastic siderite, ankerite and/or magnetite, and quartz, with rare pyrrhotite. Layering is interpreted to represent sedimentary bedding (S_0) (Ladeira, 1980; Vieira, 1987a; Junqueira, 1997). However, due to strong modification of the original features by shearing, the present mineralogical banding of the BIF is considered to be metamorphic in origin by Lobato et al. (2001a). With the onset of shear-related hydrothermal alteration, there is general replacement of metamorphic minerals and vein filling, with increase in grain size. A decrease in the abundance of magnetite is accompanied by development of ankerite. Deformed, xenoblastic, fine-to medium-sized pyrrhotite crystals grew at the expense of carbonate and magnetite (Fig. 9E). Textural relationships indicate that poikiloblastic pyrrhotite has replaced both original siderite and hydrothermal ankeritic carbonate. Although less abundant, euhedral to anhedral arsenopyrite and pyrite (±chalcopyrite) have developed at the expense of carbonate and pyrrhotite; pyrite is also partly replaced by arsenopyrite (Fig. 9F). Narrow bands of muscovite, euhedral albite crystals and rarer chlorite flakes are associated with pyrrhotite-rich gold ore. Subhedral pyrite and arsenopyrite constitute trails within BIF layers.

5.3. Geochemistry of selected wall rocks and their alteration products

Whole rock geochemical analyses were performed at the GEOLAB/GEOSOL laboratories in Belo Horizonte, Brazil. The oxides SiO_2, Al_2O_3, Fe_2O_3, CaO, MgO, TiO_2, P_2O_5, Na_2O, K_2O, MnO, Cr_2O_3, NiO and trace elements Sc, V, Cr, Co, Ni, Ba, Sr, Y, Zr, S, Cl were determined by X-ray fluorescence (Phillips, model PW1480) using glass beads and press pellets, respectively. Rare earth elements (REE) were obtained by inductively coupled plasma atomic emission spectrometry (ICP-AES). Different methods were applied when using an atomic absorption to analyze Cu, Pb, Zn, Ag, Mo, Au and As.

Average geochemical data and some selected element ratios of metabasalts and ultramafic schists samples from each of the alteration zones are presented in Tables 7 and 8, respectively. The REE patterns of metabasalt and its alteration products (Fig. 11A) suggest a tholeiitic protolith. There is an overall depletion of REE with progressive alteration, and development of a discrete to

Table 7
Compositions of metabasalts of the Raposos deposit (Junqueira, 1997) compared to TH2 Archean tholeiites (after Condie, 1976c, in Condie, 1981)

	1 (3 samples)	2	3 (2 samples)	4 (3 samples)	5 (3 samples)	TH2
	Pre-alteration zone	Chlorite zone	Chlorite–muscovite zone	Carbonate–albite zone	Carbonate–muscovite zone	Archean tholeiites
SiO_2	53.33	52.00	42.30	44.33	38.63	49.5
TiO_2	0.58	0.56	0.59	0.54	0.46	1.49
Al_2O_3	13.13	12.10	13.90	12.47	11.10	15.2
Fe_2O_3	2.13	0.73	5.70	2.29	1.41	2.80
FeO	5.60	7.30	6.70	5.07	6.63	9.17
MgO	6.83	7.30	8.85	6.07	6.80	6.82
CaO	8.43	7.40	6.90	9.07	10.57	8.79
Na_2O	3.03	2.20	0.16	2.30	0.55	2.70
K_2O	0.06	0.04	1.57	1.90	2.87	0.69
P_2O_5	0.07	0.05	0.00	0.06	0.06	0.17
MnO	0.18	0.15	0.15	0.16	0.19	0.18
H_2O	1.46	3.33	3.41	0.66	0.61	2.04
LOI	6.12	9.40	12.42	15.01	19.97	–
Total	99.58	99.31	99.33	99.32	99.30	97.33
CaO/Al_2O_3	0.64	0.61	0.50	0.73	0.95	0.58
FeO/Fe_2O_3	2.6	10	1.2	2.2	4.7	3.3
MgO/FeO	1.22	1	1.32	1.20	1.02	0.74
Cr	293	353	463	235	315	250
Ni	108	129	116	73	77	125
V	173	183	226	195	176	365
Co	56	53	66	44	47	55
Cu	67	64	144	67	45	100
Zn	84	123	148	67	96	120
Ag	2	2	2	2	2	–
As	52	35	223	362	416	–
Zr	80	78	65	71	56	135
Ba	28	40	420	303	401	90
Sr	195	124	86	139	132	190
La	9.8	8.5	4.4	6.7	4.9	13
Ce	22	18	11	17	11	30
Nd	11	8.3	4.8	8.8	6.2	17
Sm	2.2	1.9	1.1	1.7	1.3	4.0
Eu	0.6	0.37	0.25	0.46	0.37	1.3
Gd	2.1	1.6	0.96	1.6	1.3	3.8
Dy	2.3	1.9	1.3	1.6	1.6	4.2
Ho	0.45	0.37	0.27	0.32	0.33	–
Er	1.2	1.0	0.78	0.87	0.97	2.3
Yb	0.89	1.0	0.81	0.74	0.83	2.2
Lu	0.10	0.15	0.12	0.10	0.12	0.38
Y	11	7	8	10	6	30
Ni/Co	2	2.4	1.7	1.6	1.6	2.3
Zr/Y	7.3	11	8.1	7.1	9.3	4.5
$(La/Sm)_N$	2.78	2.8	2.47	2.46	2.38	2.04
Eu/Eu*	0.8	0.6	0.7	0.8	0.9	1.0
$(Yb/Gd)_N$	0.51	0.8	1.04	0.56	0.79	0.71

N=chondrite-normalized ratio (values after Taylor and McLennan, 1985).
Oxides in wt.%, trace elements in ppm. The degree of hydrothermal alteration increases from left (1) to right (5).

pronounced Eu anomaly (feldspar-poor rocks). The distribution of trace elements (Fig. 11B) shows similarity to the TH2-type tholeiitic basalts presented by Condie (1981), especially with respect to their Co, Cr, Ni and Sr values.

The REE patterns of ultramafic schists displaying varying intensities and stages of alteration (Fig. 12A) suggesting that alteration has mobilized the light REE (LREE). High Cr, Ni, Mg contents and Ni/Co ratios, and low Zr, Y and Ti contents (Fig. 12B) are

Table 8
Compositions of ultramafic schists of the Raposos deposit (Junqueira, 1997) compared to Archean spinifex-textured peridotitic komatiite (STPK) lavas and peridotite (Condie, 1981)

	1	2 (4 samples)	3	4 (2 samples)	5 (2 samples)	STPK	Peridotite
	Pre-alteration zone	Talc–chlorite zone	Chlorite–carbonate zone	Carbonate–albite zone	Carbonate–muscovite zone	Abitibi belt, Canada	Average garnet peridotite nodule from kimberlite
SiO_2	44.20	43.18	43.70	32.70	36.85	42.9	44.70
TiO_2	0.22	0.26	0.21	0.20	0.21	0.36	0.20
Al_2O_3	8.40	7.93	7.50	8.00	7.75	7.46	3.23
Fe_2O_3	1.50	1.39	1.40	0.54	1.84	2.9	1.66
FeO	7.90	6.43	5.80	5.45	5.70	6.50	7.58
MgO	20.00	22.07	12.60	11.05	10.60	24.0	39.71
CaO	7.40	5.63	9.30	14.25	12.80	7.21	2.38
Na_2O	0.08	0.17	0.09	3.15	0.63	0.13	0.27
K_2O	0.07	0.05	0.47	0.13	1.59	0.06	0.07
P_2O_5	<0.05	<0.05	<0.05	<0.05	<0.05	0.02	0.03
MnO	0.14	0.12	0.21	0.34	0.24	0.22	0.13
H_2O	4.45	2.52	2.76	1.55	1.40	6.0	0.10
LOI	8.58	11.83	17.83	23.11	21.08	–	–
Total	98.95	99.46	99.34	99.21	99.54	97.76	100.06
CaO/Al_2O_3	0.88	0.71	1.24	1.78	1.65	0.97	0.74
FeO/Fe_2O_3	5.27	4.62	4.14	10.28	3.10	2.20	4.6
MgO/FeO	2.53	3.43	2.17	2.03	1.86	3.7	5.2
Al_2O_3/TiO_2	38.18	30.5	35.71	39.02	36.90	21	16
Cr	2846	2638	1410	1928	1582	2700	2500
Ni	888	534	464	792	256	1300	2500
V	162	150	156	132	120	170	50
Co	27	68	23	36	42	110	100
Cu	5	7	45	46	56	89	30
Zn	180	101	192	66	96	90	33
As	747	738	362	1333	825	–	–
Sr	37	52	160	259	171	–	–
Zr	24	35	33	35	38	35	40
Ba	<10	21	124	148	296	–	–
La	1.9	2.2	3.6	2.8	2.0	0.45	1.3
Ce	4.4	4.7	6.9	5.4	4.6	1.18	2.9
Nd	1.8	2.2	2.5	2.4	2.3	1.33	1.6
Sm	0.62	0.42	0.54	0.55	0.51	0.45	0.32
Eu	0.18	0.14	0.13	0.16	0.16	0.21	0.10
Gd	0.82	0.49	0.48	0.45	0.65	0.50	0.29
Dy	0.69	0.75	0.48	0.67	0.86	–	–
Ho	0.14	0.16	0.11	0.15	0.18	–	–
Er	0.39	0.51	0.33	0.44	0.52	0.41	0.11
Yb	0.37	0.52	0.32	0.46	0.44	0.88	0.07
Lu	0.052	0.068	0.035	0.062	0.066	0.08	0.01
Y	6	<1	6	6	3	10	1
Ni/Co	32.89	7.85	20.17	21.99	6.09	12	25
Ti/Zr	55.00	44.57	38.18	35.65	33.16	62	30
Zr/Y	4	35	5.5	6.27	12.67	3.5	40
Ti/V	8.15	10.40	8.08	9.35	10.5	13	24
$(La/Sm)_N$	1.90	3.23	4.16	3.19	2.53	0.56	2.56
Eu/Eu*	0.77	1.02	0.77	0.93	0.87	1.3	1.00
$(Yb/Gd)_N$	0.55	1.29	0.81	1.28	0.83	2.17	0.30

N=chondrite-normalized ratio (values after Taylor and McLennan, 1985).
Oxides in wt.%, trace elements in ppm. The degree of hydrothermal alteration increases from left (1) to right (5).

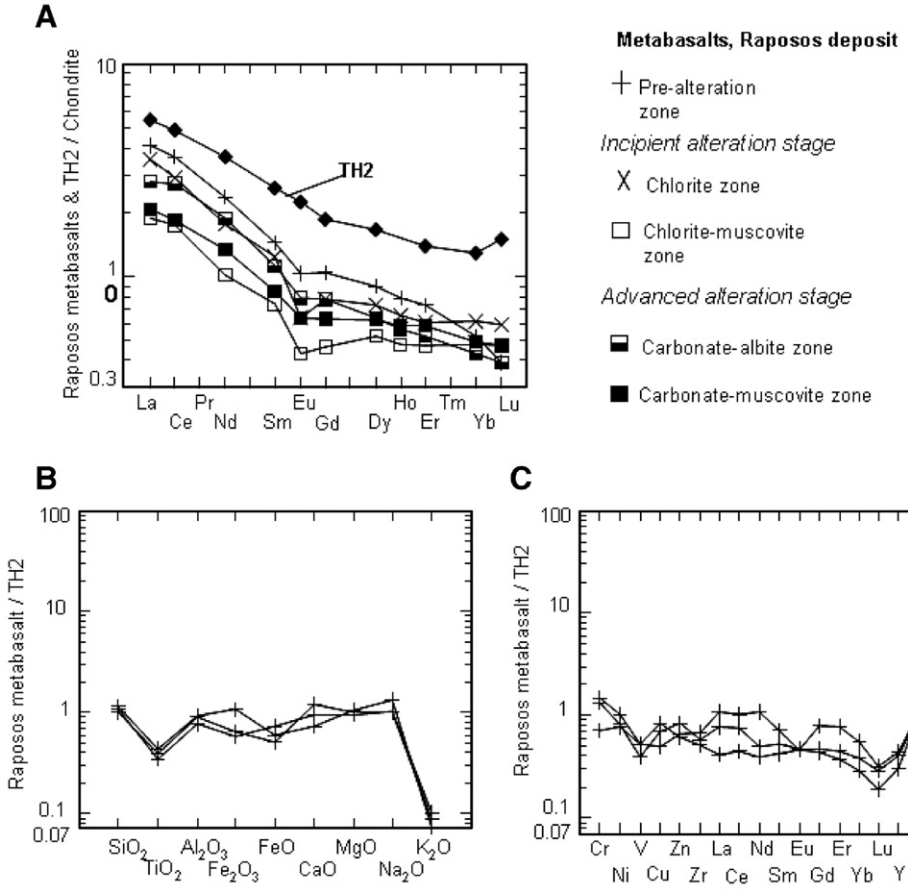

Fig. 11. A) Chondrite-normalized rare earth elements (REE) distribution of metabasalts, at varying alteration stages; the TH2 tholeiite (after Condie, 1981) is shown for comparison. Chondrite values after Sun and McDonough (1989, in Minpet, 1995). B) and C) TH2-normalized samples of the least-altered metabasalts respectively for major and trace elements.

similar to those of peridotitic komatiite (Arndt et al., 1977).

The shale-normalized REE pattern for BIF (Fig. 13) has a strong Eu positive anomaly and does not display any significant variation in the LREE and HREE trends. The Eu anomaly of the Raposos BIF, which is maintained throughout the alteration, suggests that it was formed proximal to an exhalative hydrothermal source on the ocean floor (Dymek and Klein, 1988). This corroborates the findings of Ladeira et al. (1991).

Lithogeochemical studies are also used to addresses the progression of the hydrothermal alteration through the use of the $CO_2/(CaO+FeO+MgO)$ ratio, which varies from 0.24 to 0.82 in metabasalts and from 0.14 to 0.77 in the metamorphosed ultramafic schists (Fig. 7; Junqueira, 1997). This ratio is similar for each one of the four hydrothermal alteration zones of both protholiths (Fig. 7).

The hydrothermal alteration of metabasalt involves progressive loss of Na_2O, Fe_2O_3 and ΣREE. There is addition of K_2O, and subordinate CO_2. Whereas H_2O is mainly enriched in the incipient stage of alteration, it is depleted in the advanced stage. The Fe^{2+}:Fe^{3+} ratio increases, and there is a pronounced increase in As and Ba. Leaching of Na_2O in the chlorite–muscovite zone is related to albite consumption in favor of muscovite formation. TiO_2, V, Co and Zr have little or no change as in other mesothermal gold deposits (e.g., Condie, 1981). SiO_2 and Al_2O_3 also show a slight variation.

The main chemical changes in komatiite are the pronounced enrichments in Na_2O and/or K_2O, slight enrichment in TiO_2 in the talc–chlorite zone, and loss of Fe_2O_3, FeO, CaO or MgO. There is an increase in Ba, Sr and Zr and a slight decrease in S. Both Ni and Zn are impoverished in the talc–chlorite and carbonate–albite

zones. The REE display a behavior similar to that for the metabasalt. SiO_2, Al_2O_3 and V are essentially immobile.

An earlier investigation by Vieira (1991c) shows that development of sericite, carbonate and sulfide, and tourmaline in metabasalt, coincides with gains in K, S, CO_2, Au, As, B and Ba. In komatiite, according to this author, there is enrichment of Ca, Mn, Sr and Sc and loss

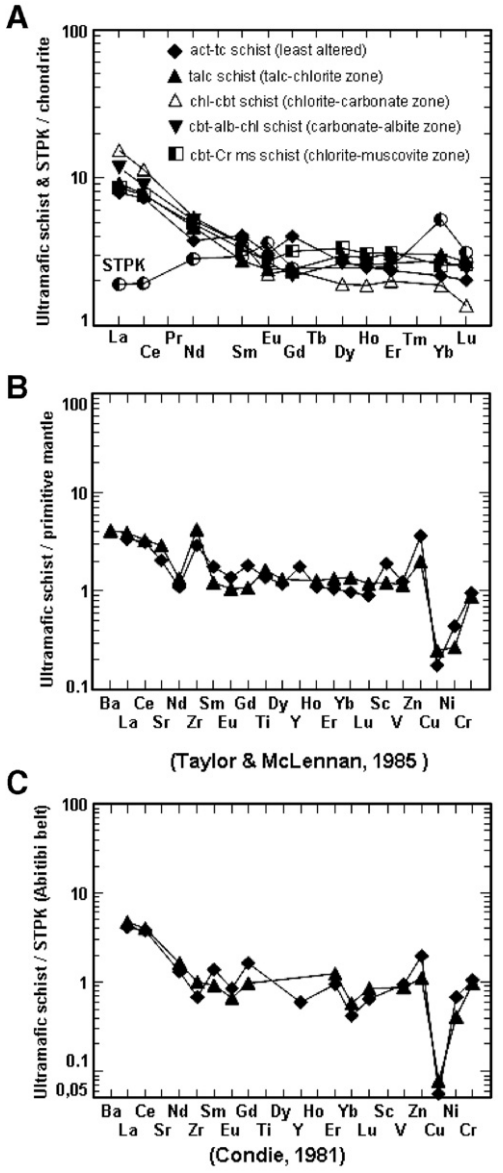

Fig. 12. A) Chondrite-normalized REE distribution of ultramafic schists at varying alteration stages; data from the Archean spinifex-textured peridotitic komatiite (STPK) lavas (Condie, 1981) is shown for comparison. Abbreviations: act — actinolite; ab — albite; cbt — carbonate; chl — chlorite; Cr ms — (Cr)-muscovite; tlc — talc. B) Primitive-mantle- and C) STPK-normalized trace elements distribution of the least-altered ultramafic schists.

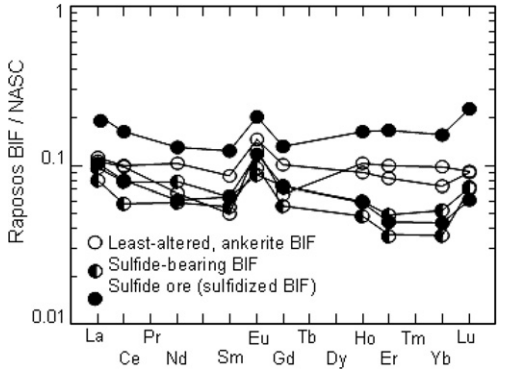

Fig. 13. REE distribution of the Raposos BIF at varying alteration stages, normalized to the North American shale composite (NASC).

of Mg, Cr, Ni and Co. Zirconium, Y, Ga, TiO_2 and Al_2O_3 show low mobility.

The alteration of BIF involved significant addition of sulfur, with contents varying from 0.41 to 5.40 wt.%. The REE values of BIF normalized to the North American Shale Composite (NASC) show that the regular, although depleted, pattern of sulfide-poor BIF is maintained, even in sulfide rich gold ores; there is a slight increase in total REE content (15.6 to 19.3 ppm).

6. Discussion and conclusions

Similar to many other gold deposits in the Nova Lima Group rocks of the QF, the Raposos gold deposit resembles Late Archean orogenic gold deposits in greenstone belts elsewhere in the world, in terms of ore characteristics (Groves et al., 1998). Wall rock alteration and ore fluid composition (Lobato et al., 1998, c) are typical of orogenic gold deposits hosted by mafic volcanic rocks and by BIF (Phillips et al., 1984).

The following conclusions can be deduced from the present contribution:

1. Mineralization at the Raposos orogenic gold deposit is associated with structurally-controlled hydrothermal alteration of BIF and its wall rocks.
2. Orebodies at Raposos are clearly associated with D_1-related shear zones in BIF. Regional studies (Vieira, 1991b) suggest that these structures are associated with EW-directed, transcurrent faults. Sulfidation of BIF and the generation of mineable gold concentrations are likely to relate to the same processes that produced the alteration assemblages in the wall rocks.
3. As suggested by the photomicrographs in Fig. 9, hydrothermal alteration overprints the metamorphic assemblages. Alteration is expressed by zones of

chlorite, carbonate and muscovite/sulfide assemblages towards the ore.

4. Rare earth and trace element patterns of the metabasalt and its alteration products suggest a tholeiitic protolith. In the case of the ultramafic schists, the precursors were possibly a peridotitic komatiite. The Eu anomaly of the Raposos BIF suggests that it was formed proximal to an exhalative hydrothermal source on the ocean floor.
5. Evidence of a consistent composition for the ore fluid is inferred by hydrothermal alteration reactions that indicate a H_2O-rich fluid containing CO_2+Na^+ and S. The distal alteration halos are dominated by hydrated silicate phases (mainly chlorite), with minor carbonates, indicating the fixation of mainly H_2O. The CO_2 is consumed to form carbonates in the intermediate alteration stage, in halos around the chlorite-dominated zones. These characteristics suggest variations in the H_2O to CO_2-ratio of the sulfur-bearing, aqueous-carbonic ore fluid, which interacted at varying fluid to rock ratios with progression of the hydrothermal alteration (Lobato et al., 2001a,c).
6. Fluid composition can also be inferred based on the existing, limited fluid inclusion data of Godoy (1994). Three types of fluid inclusions have been identified based on microthermometric and spectroscopic studies using Raman Spectroscopy. Type I inclusions are abundant in the ore and composed of H_2O, CH_4 and N_2, and a smaller proportion of CO_2. Type II occurs in tension gashes and has H_2O, CO_2 and NaCl, with lesser CH_4. Type III is an aqueous, saline fluid. Type I is interpreted as the initial, more reducing, mineralizing fluid. Type II is related to carbonate alteration (probably evolved from I), and type III to late, brittle deformation structures. The pressure and temperature of gold mineralization of 3.5 kbar and 400 °C, respectively, take into consideration type I inclusions and temperatures of formation for arsenopyrite and chlorite (Godoy, 1994).

Acknowledgements

The authors acknowledge the essential input and support of former staff at Anglo Gold Ashanti, previously known as Mineração Morro Velho. The research was funded by the Brazilian and the Minas Gerais state research foundations (Conselho Nacional de Desenvolvimento Científico e Tecnológico-CNPq and Fundação de Amparo a Pesquisa do Estado de Minas Gerais-FAPEMIG). LML is particularly indebted to CNPq for a continuing grant. Discussions with Frederico W. R. Vieira have been invaluable during the field studies. We are grateful for the careful review of the manuscript by Prof. David I. Groves. Diógenes Vial was vital in stimulating preparation of this paper.

References

Arndt, N.T., Naldrett, A.J., Pyke, D.R., 1977. Komatiitic and iron-rich tholeiitic lavas of Munro Township, northeast Ontario. Journal of Petrology 18, 319–369.

Baltazar, O.F., Pedreira, A.J., 1996. Associações litofaciológicas. In: Zucchetti, M., Baltazar, O.F. (Eds.), Projeto Rio das Velhas — Texto explicativo do mapa geológico integrado, escala 1:100,000. CPRM- Serviço Geológico do Brasil, Belo Horizonte, Brazil, pp. 43–48.

Baltazar, O.F., Zucchetti, M., 2007. Lithofacies associations and structural evolution of the Archean Rio das Velhas greenstone belt, Quadrilátero Ferrífero, Brazil: A review of the setting of gold deposits. Ore Geology Reviews 32, 471–499 (this volume).

Carneiro, M.A., Carvalho Jr., I.M., Teixeira, W., 1998. Petrologia, geoquímica e geeocronologia dos diques máficos do complexo metamórfico Bonfim setentrional (Quadrilátero Ferrífero) e suas implicações na evolução crustal do cráton São Francisco meridional. Revista Brasileira de Geociências 28 (1), 29–44.

Colvine, A.C., Fyon, A.J., Heather, K.B., Marmont, S., Smith, P.M., Troop, D.G., 1988. Archaean Lode Gold Deposits in Ontario. Toronto, Canada, Miscellaneous Paper 139, Ontario Geological Survey, 136 pp.

Condie, K.C., 1981. Archean Greenstone Belts. Developments in Precambrian Geology, vol. 3. Elsevier, Amsterdam. 434 pp.

Deer, W.A., Howie, R.A., Zussman, J., 1966. An Introduction to Rock Forming Minerals. Longmans, Group Ltd, London, England. 528 pp.

DeWitt, E., Landis, G.P., Zartman, R.E., Garayp, E., Martins Pereira, S.L., Prado, M.G.B., Vieira, F.W.R., Thorman, C.H., 1994. Isotopic and fluid inclusion data on the age and origin of the São Bento and Morro Velho Gold Deposits, Minas Gerais, Brazil. In: Thorman, C.H., Lane, D.E. (Eds.), Research on Mineral Deposits. Part A: Programs and Abstracts, 9th V.E. McKelvey Forum on Energy and Mineral Resources. United States Geological Survey Circular, vol. 1103-A, pp. 27–29.

Dorr II, J.V.N., 1969. Physiographic, stratigraphic and structural development of the Quadrilátero Ferrífero Minas Gerais. United States Geological Survey Professional Paper 641-A. 110 pp.

Dymek, R.F., Klein, C., 1988. Chemistry, petrology and origin of banded iron-formation lithologies from the 3800 Ma Isua supracrustal belt, West Greenland. Precambrian Research 39, 247–302.

Godoy, M.L.S., 1994. Evolução tectono-metamórfica da mineralização aurífera de Raposos (MG). MSc Thesis, UNESP, Instituto de Geociências e Ciências Exatas, Rio Claro, Brazil, 123 pp.

Groves, D.I., Goldfarb, R.J., Gebre-Mariam, M., Hagemann, S.G., Robert, F., 1998. Orogenic gold deposits: a proposed classification in the context of their crustal distribution and relationship to other gold deposit types. Ore Geology Reviews 13, 7–27.

Hey, M.H., 1954. A new review of the chlorites. Mineralogical Magazine 30, 277.

Junqueira, P.A., 1997. Geologia do depósito de ouro da Mina de Raposos, Quadrilátero Ferrífero, com ênfase na alteração hidrotermal. MSc Thesis, Universidade Federal de Minas Gerais, Instituto de Geociências, Belo Horizonte, Brazil, 141 pp.

Ladeira, E.A., 1980. Metallogenesis of Gold at the Morro Velho Mine and in Nova Lima District, Quadrilátero Ferrífero, Minas Gerais, Brazil. Ph.D. Thesis, University of Western Ontario. Department of Geology, London, Canada, 272 pp.

Ladeira, E.A., 1985. Metalogênese do Ouro na Mina de Morro Velho e no Distrito de Nova Lima, Minas Gerais, Brasil. In: Grossi Sad, J.H., Barcelos, A. (Eds.), Contribuições à Geologia e à Petrologia. Sociedade Brasileira de Geologia e Cia. Brasileira de Metalurgia e Mineração, Belo Horizonte, Brazil, pp. 95–151.

Ladeira, E.A., 1991. Genesis of gold in Quadrilátero Ferrífero: a remarkable case of permanency, recycling and inheritance — a tribute to Djalma Guimarães, Pierre Routhier and Hans Ramberg. In: Ladeira, E.A. (Ed.), Brazil Gold' 91. A.A. Balkema, Rotterdam, pp. 11–30.

Ladeira, E.A., Lobato, L.M., Grossi Sad, J.H., Simões, E.J.M., Vieira, F.W.R., 1991. Petrology and geochemistry of wall rocks, and of BIF-host rock to gold mineralization at level 2400' of Raposos Mine, Minas Gerais, Brazil. In: Ladeira, E.A. (Ed.), Brazil Gold '91. A.A. Balkema, Rotterdam, pp. 437–445.

Lobato, L.M., Vieira, F.W.R., 1998. Styles of hydrothermal alteration and gold mineralization associated with the Nova Lima Group of the Quadrilátero Ferrífero: part II, the Archean mesothermal gold-bearing hydrothermal system. Revista Brasileira de Geociências 28 (3), 355–366.

Lobato, L.M., Vieira, F.W.R., Ribeiro-Rodrigues, L.C., Pereira, L.M.M., Menezes, M.G., Junqueira, P.A., Martins-Pereira, S.L., 1998. Styles of hydrothermal alteration and gold mineralization associated with the Nova Lima Group of the Quadrilátero ferrífero: part I, description of selected gold deposits. Revista Brasileira de Geociências 28 (3), 339–354.

Lobato, L.M., Ribeiro-Rodrigues, L.C., Zucchetti, M., Noce, C.M., Baltazar, O.F., da Silva, L.C., Pinto, C.P., 2001a. Brazil's premier gold province. Part I: the tectonic, magmatic and structural setting of the Archean Rio das Velhas greenstone belt, Quadrilátero Ferrífero. Mineralium Deposita 36, 228–248.

Lobato, L.M., Ribeiro-Rodrigues, L.C., Vieira, F.W.R., 2001b. Brazil's premier gold province. Part II: geology and genesis of gold deposits in the Archean Rio das Velhas greenstone belt, Quadrilátero Ferrífero. Mineralium Deposita 36, 249–277.

Lobato, L.M., Ribeiro Rodrigues, L.C., Zucchetti, M., Costa, M.N. de S., Martins, R., Lehne, E., Alves, J.V., Tassinari C.C.G., Vieira, F.W.R., Biasi, E.E., Silva, R.C.F., Pereira, V.C.A., Noce, C.M., 2001. Geologia do depósito de ouro Cuiabá, Quadrilátero Ferrífero, Minas Gerais. In: Jost, H., Brod, J.A., de Queiroz, E.T. (Eds.), Caracterização de depósitos auríferos em distritos mineiros brasileiros. Departamento Nacional da Produção Mineral/Agência para o Desenvolvimento Tecnológico da Indústria Mineral Brasileira (ADIMB), Brasília, Brazil, p. 3–77.

Machado, N., Carneiro, M.A., 1992. U–Pb evidence of late Archean tectono-thermal activity in the southern São Francisco shield, Brazil. Canadian Journal of Earth Science 29, 2341–2346.

Machado, N., Schrank, A., Noce, C.M., Gauthier, G., 1996. Ages of detrital zircon from Archean–Paleoproterozoic sequences: implications for greenstone belt setting and evolution of a Tranzamazonian foreland basin in Quadrilátero Ferrífero, SE Brazil. Earth and Planetary Science Letters 141, 259–276.

Martins-Pereira, S.L., 1995. Controles litoestruturais da mineralização aurífera no distrito de Santa Bárbara, Quadrilátero Ferrífero, MG: mina São Bento. MSc Thesis, Universidade Federal de Minas Gerais, Instituto de Geociências, Belo Horizonte, Brazil, 158 pp.

Martins Pereira, S.L., Lobato, L.M., Ferreira, J.E., Jardim, E.C., 2007. Nature and origin of the BIF-hosted São Bento gold deposit, Quadrilátero Ferrífero, Brazil, with special emphasis on structural controls. Ore Geology Reviews 32, 571–595 (this volume).

MINPET 2.02, 1995. Reference manual, Minpet software for Windows v. 2.02, Québec, Canada, 263 pp.

Noce, C.M., 2001. Geochronology of the Quadrilátero Ferrífero: a review. Geonomos-Revista de Geociências 8 (1), 15–23.

Noce, C.M., Tassinari, C.C.G., Lobato, L.M., 2007. Geochronological framework of the Quadrilátero Ferrífero, with emphasis on the age of gold mineralization hosted in the Archean greenstone belt. Ore Geology Reviews 32, 500–510 (this volume).

Oliveira, G.A.I., Clemente, P.C., Vial, D.S., 1983. Excursão à Mina de Ouro de Morro Velho. Anais do Simpósio de Geologia de Minas, 2, vol. 3, pp. 497–505.

Pereira, L.M.M., 1996. Estudo da Alteração Hidrotermal do Corpo SE-2, nível 5 da mina de ouro de Juca Vieira, Quadrilátero Ferrífero, MG. MSc Thesis, Universidade Federal de Minas Gerais, Instituto de Geociências, Belo Horizonte, Brazil, 204 pp.

Phillips, G.N., Groves, D.I., Martyn, J.E., 1984. An epigenetic origin for Archean banded iron-formation-hosted gold deposits. Economic Geology 79, 162–171.

Ramsay, J.G., 1967. Folding and Fracturing of Rocks. McGraw-Hill Book Co., New York. 568 pp.

Ribeiro-Rodrigues, L.C., 1998. Gold in Archaean banded iron-formation of the Quadrilátero Ferrífero, Minas Gerais, Brazil — the Cuiabá Mine. Aachener Geowissenschaftliche Beiträge, Band 27. 264 pp.

Ribeiro-Rodrigues, L.C., Oliveira, C.G., Friedrich, G., 2007. The Archaean BIF-Hosted Cuiabá Gold Deposit, Quadrilátero Ferrífero, Minas Gerais, Brazil. Ore Geology Reviews 32, 543–570 (this volume).

Taylor, S.R., McLennan, S.M., 1985. The Continental Crust: Its Composition and Evolution. Blackwell, Oxford. 312 pp.

Tolbert, G.E., 1964. Geology of the Raposos Gold Mine, Minas Gerais, Brazil. Economic Geology 49, 775–798.

Vial, D.S., 1980. Geologia da Mina de Ouro de Raposos. Anais Congresso Brasileiro Geologia, vol. 3. Sociedade Brasileira de Geologia, Camboriú, Brazil, pp. 1851–1866.

Vial, D.S., DeWitt, E., Lobato, L.M., Thorman, C.H., 2007. The geology of the Morro Velho gold deposit in the Archean Rio das Velhas greenstone belt, Quadrilátero Ferrífero, Brazil. Ore Geology Reviews 32, 511–542 (this volume).

Vieira, F.W.R., 1987a. Novo contexto geológico para a mina de Raposos. Anais do Simpósio de Geologia de Minas Gerais, 4. Boletin, vol. 7. Sociedade Brasileira de Geologia, Belo Horizonte, Brazil, pp. 343–357.

Vieira, F.W.R., 1987b. Gênese das mineralizações auríferas da mina de Raposos. Anais do Simpósio de Geologia de Minas Gerais, 4. Boletin, vol. 7. Sociedade Brasileira de Geologia, Belo Horizonte, Brazil, pp. 358–367.

Vieira, F.W.R., 1988. Processos epigenéticos de formação dos depósitos auríferos e zonas de alteração hidrotermal do Grupo Nova Lima, Quadrilátero Ferrífero, Minas Gerais. Anais Congresso Brasileiro Geologia, 35, vol. 1. Sociedade Brasileira de Geologia, Belém, Brazil, pp. 76–87.

Vieira, F.W.R., 1991a. Textures and processes of hydrothermal alteration and mineralization in the Nova Lima Group, Minas Gerais, Brazil. In: Ladeira, E.A. (Ed.), Brazil Gold '91. A.A. Balkema, Rotterdam, pp. 319–325.

Vieira, F.W.R., 1991b. Petrologia e litogeoquímica do setor W do greenstone belt Rio das Velhas, MG. AMSA's First Internal Geology Symposium. Mineração Morro Velho S.A, Nova Lima, Brazil. 24 pp.

Vieira, F.W.R., 1991c. Gênese das mineralizações auríferas do setor W do greenstone belt Rio das Velhas, MG. AMSA's First Internal

Geology Symposium. Mineração Morro Velho S.A, Nova Lima, Brazil. 18 pp.

Vieira, F.W.R., 2000. Relationships between tectonic structures and auriferous mineralization of the Nova Lima Group. Unpublished report, Mineração Morro Velho Ltda., Nova Lima, Brazil, 18 pp.

Vieira, F.W.R., Oliveira, G.A.I., 1988. Geologia do distrito aurífero de Nova Lima, Minas Gerais. In: Schobbenhaus, C., Coelho, C.E.S. (Eds.), Principais Depósitos Minerais do Brasil. Metais Básicos não Ferrosos, Ouro e Alumínio, vol. 3. Departamento Nacional da Produção Mineral, Brasília, Brazil, pp. 377–391.

Vieira, F.W.R., Simões, E.J.M., 1992. Geology of the Nova Lima area and excursion to the Raposos mine. In: Gold Deposit Modeling Course. International Union of Geological Sciences/ UNESCO, p. 1–24.